Cost-Optimal Design of a Household Batch Electrodialysis Desalination Device

by

Sahil R. Shah

Submitted to the Department of Mechanical Engineering
in partial fulfillment of the requirements for the degree of

Master of Science in Mechanical Engineering

at the

MASSACHUSETTS INSTITUTE OF TECHNOLOGY

June 2017

Signature redacted

Author .....
Department of Mechanical Engineering
May 15, 2017

Signature redacted

Certified by .....
Amos G. Winter, V
Assistant Professor of Mechanical Engineering
Thesis Supervisor

Signature redacted

Accepted by .....
Rohan Abeyaratne
Professor of Mechanical Engineering

Cost-Optimal Design of a Household Batch Electrodialysis Desalination Device

by

Sahil R. Shah

Submitted to the Department of Mechanical Engineering
on May 15, 2017, in partial fulfillment of the
requirements for the degree of
Master of Science in Mechanical Engineering

Abstract

This thesis investigates the pareto-optimal design of a household point-of-use batch electrodialysis (ED) system to provide a cost-effective replacement for existing reverse osmosis (RO) devices, for brackish water desalination of Indian groundwater, at lower energy consumption and higher recovery: 80-90% vs 25-40%. Target specifications derived from user-interviews, and RO products, guided the selection of a batch architecture, for which a coupled flow-mass transport model to predict desalination rate was developed, and validated using a lab-scale ED stack. The effects of varying the production rate (9-15 L/hr) and product concentration (100-300 mg/L) requirements on optimal selection of geometry, flow-rates, and applied voltage for total cost minimization were then explored using a multi-objective genetic algorithm. Given the low utilization of the system and the current cost of materials, the energetic cost was dominated by the capital-cost of the system. At a fixed feedwater concentration of 2000 mg/L, which is representative of the upper bound on groundwater salinity underlying much of India, and a recovery ratio of 90%, the capital cost sharply increased for systems targeted at 100 mg/L vs 200 mg/L and 300 mg/L: \$141, \$93, and \$79, respectively averaged for systems that produced between 11.5 and 12.5 L/hr of desalinated water. Promising directions for additional cost reduction include voltage-regulation during the batch process and the development of inexpensive pumps. In addition, a candidate cost-optimal design was prototyped and tested to verify that the measured desalination performance agreed with the modeled expectations.

Thesis Supervisor: Amos G. Winter, V
Title: Assistant Professor of Mechanical Engineering

Acknowledgments

I owe my sincerest appreciation to the following individuals for playing an instrumental role in the completion of this work.

- My family, for their love and unwavering support.
- Amos, for challenging me with meaningful problems, and inspiring me to develop impactful solutions.
- David, Sterling, and Natasha, for providing invaluable input, generous assistance, and detailed critique.
- Scott, for being a brilliant UROP.
- Dr. Kumar, Dr. Sankar, Dr. Venkatesh, and Dr. Rao, at Eureka Forbes and Aquadiagnostics, for their feedback and hospitality during my visits to India.
- Nevan, Chintan, and Rob, for their guidance and mentorship.
- My colleagues at the GEAR Lab, for engaging in exciting research and motivating me to do the same.
- My friends, especially Emily, for the laughter and adventures that we have shared together.
- And all of the individuals and families in India who have invited me into their homes, and shared their experiences.

I am also grateful to the following institutions for providing funding to support this work:

Tata Center for Technology and Design

Eureka Forbes Ltd.

MIT Undergraduate Research Opportunities Program

THIS PAGE INTENTIONALLY LEFT BLANK

Contents

THIS PAGE INTENTIONALLY LEFT BLANK

List of Figures

List of Tables

THIS PAGE INTENTIONALLY LEFT BLANK

Chapter 1

Introduction

This thesis investigates the design of a point-of-use batch electrodialysis (ED) system to provide a higher-recovery yet cost-effective replacement for existing reverse osmosis (RO) devices, which are used for desalination of groundwater in Indian households. In this work, I have

- identified design requirements for the proposed ED-based system,
- developed and validated models for analyzing flow and mass transfer through the ED stack,
- investigated cost-optimal design configurations targeted at varying production requirements using simulation,
- fabricated and tested a prototype system intended for the household application,
- and, suggested promising research directions for further cost reduction.

1.1 The Problem

The WHO UNICEF Joint Monitoring Programme for Water Supply and Sanitation reported that 94% of the urban population in India had access to an *improved source* of drinking water in 2015 [1]. However, in 2011, 13-32% *improved sources* tested in five countries returned contamination levels unsafe for drinking, thereby indicating

that an *improved source* does not guarantee clean water [2]. Similarly, water testing in India has also indicated that water quality remains problematic in Indian cities. As high as 70% of tap-water samples in certain municipal wards of Mumbai tested as having unsafe levels of bacterial contamination, and municipal supply samples in Jaipur and Calcutta also raised similar concerns [3]. In 2016, Ghosh *et al.* found that 80% of surveyed Delhi respondents in organized housing did not consider their municipal water to be reliable for drinking [4], indicating that the public is aware of the risks associated with drinking it.

Compounding the issue of poor quality is the inadequate and intermittent supply of municipal water. Sixty five percent of the 2734 households surveyed by Shaban and Sharma in Delhi, Kanpur, Kolkata, Ahmedabad, Mumbai, Hyderabad and Madurai were considered water-deficient, receiving less than 100 liters per capita per day [5], and only 18% received 24-hour water supply. Given the insufficient municipal supply, households rely on groundwater to accommodate their water needs. Shaban and Sharma determined that while only 7% of households depended solely on groundwater, an additional 38% used groundwater to supplement their piped supply [5]. In a wider study spanning more cities, Bajpai and Bhandari estimated that approximately 28% of urban homes depended on groundwater [6] as their main source of water.

However, much of the groundwater underlying India is also unsafe for drinking without treatment. While the content of microbiological pathogens is lower than in surface water [7], other contaminants affecting its quality include nitrates, iron, arsenic, fluoride, and salinity [8]. In a study performed by the Central Ground Water Board, groundwater that underlies 60% of India was classified as being brackish (Fig.1-1). Water from these sources was characterized as having high salt content with total dissolved solids (TDS) ranging from 480 mg/L to 3000 mg/L. This salinity exceeds the 500 mg/L TDS standard recommended by the Bureau of Indian Standards (BIS) for drinking water [9], and is indicative of poor palatability. The consumption of high salinity water may also pose adverse health effects including gastro-intestinal irritation [9] and the development of kidney stones [10].

Complicating matters further, domestic consumption, together with industrial

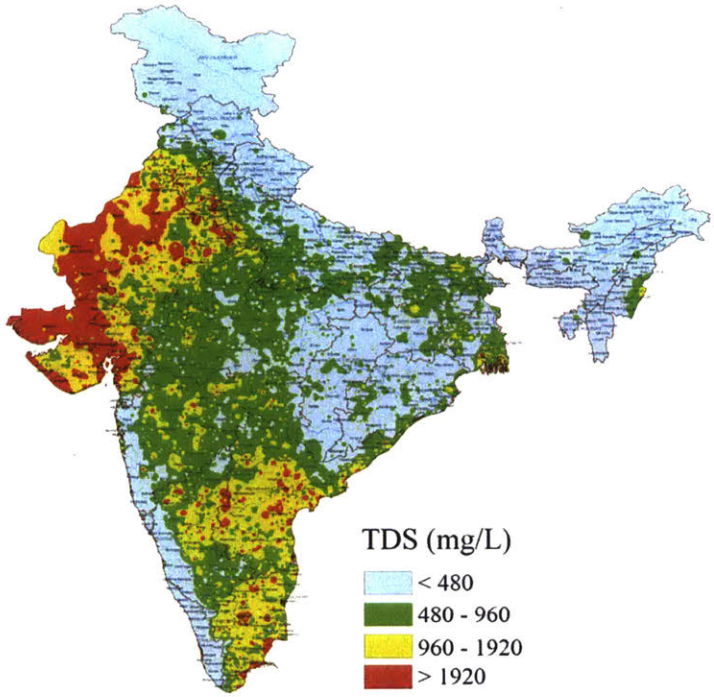

Figure 1-1: Groundwater salinity map of India [11].

and agricultural exploitation of groundwater has resulted in depletion of the resource [12, 13] (Fig.1-2). Of the 5723 blocks assessed by the Central Groundwater Board in 2010, 839 were found to be over-exploited, 550 were classified as critical, and 550 were determined to be in a semi-critical state [11, 14]. With more than 60% of irrigated agriculture and 85% of drinking water supplies dependent on groundwater in India [13], it is prudent the remaining resources be conserved and better-managed.

1.1.1 Existing Use of Reverse Osmosis Systems

Since the existing public infrastructure is unable to reliably deliver safe, desalinated, and uncontaminated water to homes, consumers have turned to in-home water purification. However, methods which include straining water though a cloth, boiling, or ultraviolet (UV), treatment do not address the high levels of dissolved salts present in groundwater. The only commercially available household water treatment option in India that is capable of managing this salinity is reverse osmosis (RO). In RO, a mechanical pressure is applied to overcome the osmotic pressure and drive water

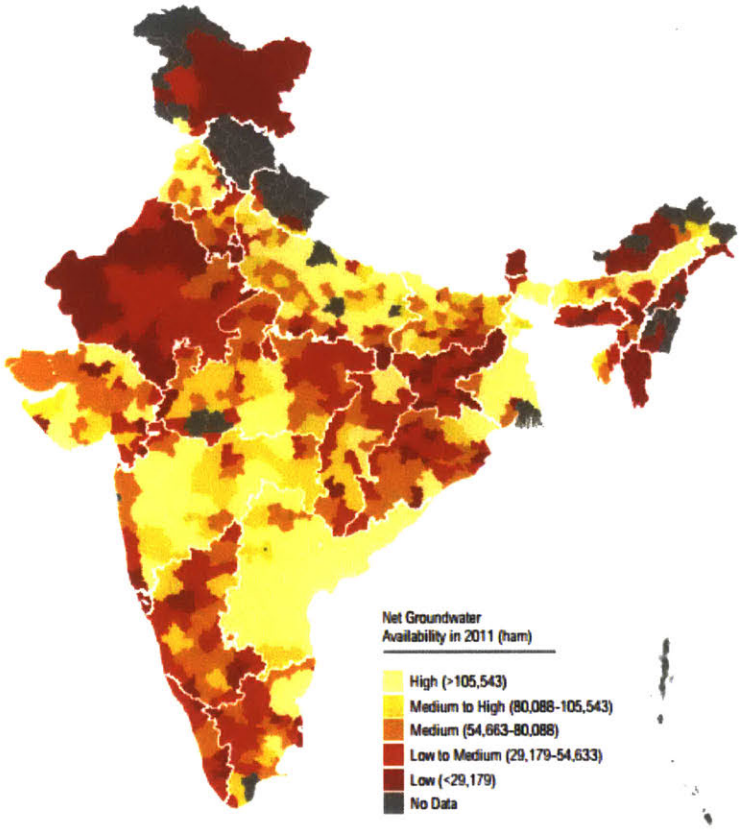

Figure 1-2: Map of groundwater availability across India, generated using India Water Tool [15], using data provided by the Central Groundwater Board. The net annual groundwater availability is defined as the available groundwater after deducting the natural discharges to the surface, during the non-monsoon period, from the annual replenishable groundwater due to rainfall.

across a semi-permeable membrane, against a concentration gradient, from a high salinity solution to one of lower salinity.

Household RO systems are widely used in Indian homes for desalination and water purification. The scale addressed here refers to point-of-use (POU) household water treatment and storage systems that typically produce 8-15 L/hr of drinking water, store 7-10 L, weigh 8-11 kg, and are usually wall-mounted or placed on kitchen counters in individual homes (Fig.1-3). These systems are capable of desalinating groundwater to a total dissolved salt (TDS) content that is suitable for drinking (less than 500 mg/L [9]), but they recover only 25-40% [18] of the feed, thereby further stressing the limited water resources. O'Connor estimates that even at an assumed

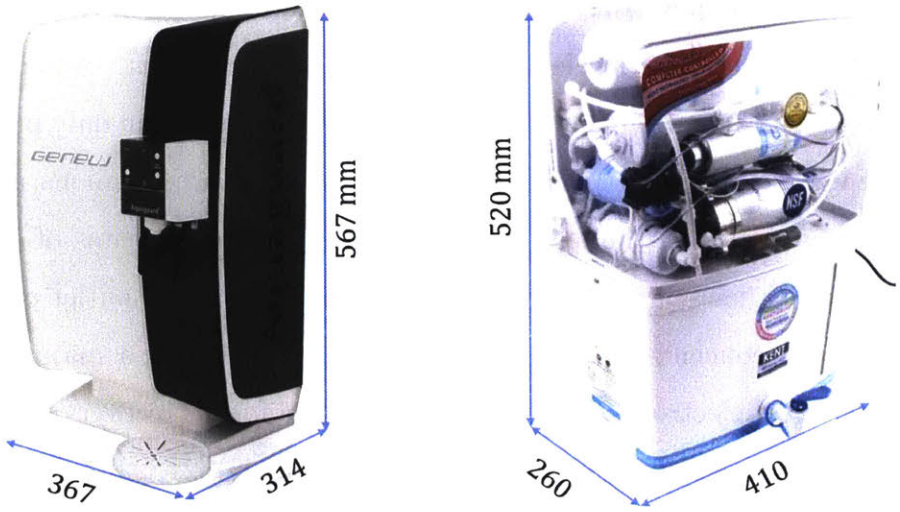

Figure 1-3: Two popular RO purifier in the Indian market, with their respective dimensions: Aquaguard Geneus by Eureka Forbes Ltd. [16] (*left*), and Grand RO Plus by Kent [17] (*right*).

conservative RO adoption rate of 30% among households in the top two socioeconomic tiers, a total of 390 million liters of water per day is lost as reject in Indian cities to satisfy drinking water needs [19]. Given this significant wastage, an alternative device is sought to provide the same desalination capability, while conserving more water.

The demand for POU home-treatment RO devices has grown significantly since their introduction in 1999. In a survey of 496 Delhi homes conducted by Ghosh *et al.* in 2016, it was found that 77% and 44% of high and middle-income group households, respectively, had adopted RO water treatment systems [4]. Furthermore, the market for these products is forecast to continue growing at a compound annual growth rate of 18.2% between 2016 and 2024 [20]; therefore, there is also a commercial opportunity for more efficient desalination solutions to capture a fraction of this demand.

1.2 Electrodialysis, a viable alternative

Electrodialysis (ED) is an alternative desalination process to RO, whereby saline water flows through a series of channels in a stack (Fig.1-4). An electric potential is applied across the stack, using electrodes, to force the movement of anions towards

the anode and cations move towards the cathode. The channels in the ED stack are separated by alternating permselective ion-exchange membranes. Anions can only pass through anion exchange membranes (AEM), while cations can only pass through cation exchange membranes (CEM). This selective transport of anions and cations results in the separation of the feed solution into alternating streams of diluted and concentrated saline flows, which are individually collected at the outlet of the stack.

Given that the concentration of the groundwater underlying a majority of India is under 2000 mg/L, electrodialysis (ED) can provide a higher recovery (80-90%) and more energy-efficient desalination compared to RO (Fig1-5) [21, 22]. ED desalination may not provide significant energy savings alone, considering only approximately 7.5% of the total household energy consumption is related to water purification [4]; however, together with pumping less water to roof-top tanks (37.5% of total [4]), the energy savings could be significant. In addition to higher recovery and energy-efficiency, ED is also known to have a number of other benefits over RO including longer membrane life, lower vulnerability to feed water changes, operation at higher temperatures, and lower sensitivity to chlorine [22, 23].

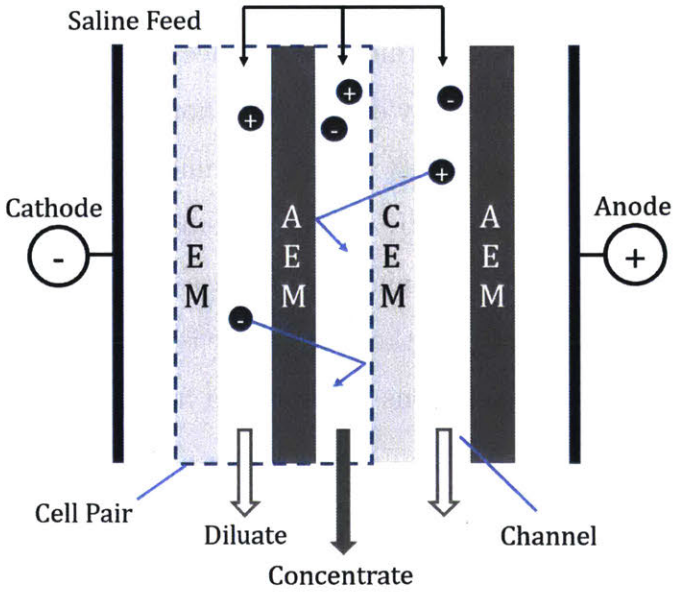

Figure 1-4: In ED, a voltage potential is applied across a series of alternating cation (CEM) and anion (AEM) exchange membranes to draws ions from the diluate to the concentrate channels.

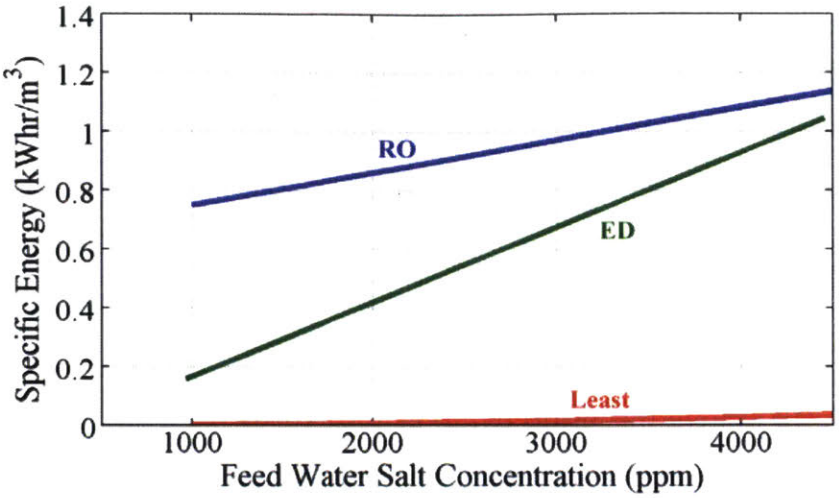

Figure 1-5: Wright and Winter compared the specific energy for desalination between ED and RO for varying feedwater concentration, and a product water concentration of 350 mg/L. Recovery ratios of 80% and 50% were assumed for batch ED and RO, respectively, with the latter operating at an overpressure of 8 bar and 75% pump efficiency [21]. ED was found to consume less energy in the groundwater salinity range prevalent in India.

The primary disadvantage of ED in this comparison is that, RO is also capable of removing pathogenic organisms from the water. However, existing domestic RO water purification systems are also equipped with pre-treatment and post-treatment steps that manage this microbiological content, including ultrafiltration and UV disinfection.

Equipped with similar pre and post-treatment, an ED-based POU household water treatment system has the potential to satisfy the desalination and purification needs of Indian households while providing a higher recovery and consuming less energy than RO. Similarly, growing concern over water scarcity and the need for more energy-efficient desalination has also recently revived an interest in the possibility of using ED for brackish water desalination and tap-water softening in European cities [24].

Despite this interest surrounding the use of ED for household water treatment purposes, little work has been performed to characterize the design of an appropriate ED system for the application. Pilat developed and piloted more than 200 domestic ED units before 2001, but little information regarding cost or the design of the system was provided [25]. More recently, Thampy *et al.* investigated a hybrid approach

whereby ED was used to initially desalinate 2000-4000 mg/L water to 500 mg/L and further desalination to 120 mg/L or lower thereafter was achieved using RO [26]. Given that their small-scale system operated in a continuous process, without the recirculation of product water, only 50-60% of the feed supply was recovered. Instead, Nayar *et al.* showed that it was feasible to implement ED solely in a batch architecture, where product water is recirculated, to desalinate from 3000 mg/L to 350 mg/L, at a competitive production rate of 12 L/hr while providing 80% recovery [27]. However, the system was projected to be too expensive for the given application: $206 for the entire system, $138 of which was attributed to the ED stack and pumps.

It follows that the proposed batch ED desalination system needs to be redesigned for lower cost in order to be competitive with RO. This objective forms the central topic of this thesis.

1.2.1 System Specifications

Target specifications for the proposed ED-based household water treatment system were derived from the performance offered by existing RO products, interviews with users of household water-treatment systems, and input from our collaborator, Eureka Forbes Ltd (Table 1.1).

Table 1.1: Household ED Desalination Treatment Specifications

Specification	Target
Feed Concentration	2000 ppm
Product Concentration	100 ppm
Desalination Rate	9-15 L/hr
Recovery Ratio	90%
Manufacturing Cost	$75
Packaging	Similar envelope as existing RO devices
Storage Capacity	8-10 L

It is worthwhile noting that the World Health Organization (WHO) [28] and Bureau of Indian Standards [9] consider water with total dissolved salt (TDS) content that is less than 500 mg/L to be safe for drinking. However, product water concentrations as low as 100 mg/L are targeted in this work in order to conform to the palette

of Indian customers who are accustomed to drinking RO-filtered water [26].

1.2.2 Proposed System Architecture

ED can be implemented in two distinct architectures: batch and continuous. The batch process involves recirculation of both the diluate and concentrate streams through the stack until the salt concentration in the diluate tank decreases to the desired level, whereas the desired diluate salinity is achieved within a single pass of the feed through the stack in a continuous process (Fig.1-6).

Although a continuous architecture would allow for instant water desalination and simpler plumbing, the size of such a system would be prohibitively large for household application. In contrast, the batch architecture is better suited here, given that the proposed system is required to fit within a similar envelope as existing RO devices (Fig.1-3). Furthermore, since recirculation allows a smaller stack to be used than for a comparable continuous process, the capital cost of the treatment system is also decreased. Therefore, a batch architecture was selected for the proposed ED-based household water treatment system.

The batch ED system (Fig.1-6 *right*) evaluated by Nayar *et al.*[27] and developed further in this thesis consists of two primary flow circuits: one for the diluate, and the other for the concentrate. At the start of each batch process, both tanks hold feedwater at the same concentration. The relative volume of water in the diluate versus the concentrate circuits governs the recovery ratio of the process. During desalination, a voltage is applied and fluid is recirculated through the stack until the desired concentration is achieved in the diluate tank. At the end of the batch process, the diluate is drained into a separate storage tank for on-demand delivery to the user. With this architecture, treatment duration can easily be adopted to accommodate varying feedwater salinity and product water salinity preferences.

An additional circuit may be required to rinse the electrodes; however, this stream does not affect desalination performance significantly, and could potentially be integrated with the concentrate stream [26].

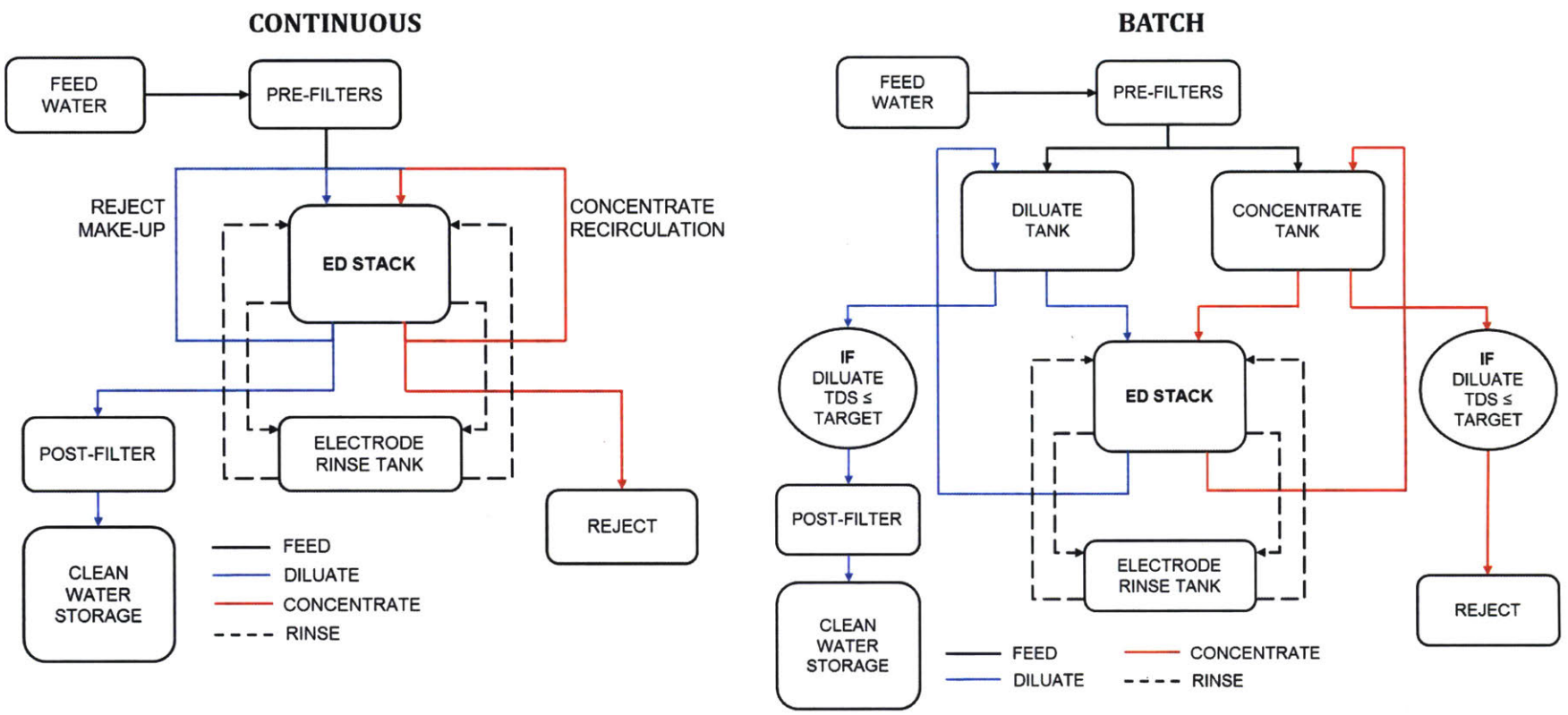

Figure 1-6: Comparison of a continuous (*left*) and batch (*left*) ED processes. Desalination to the target diluate is performed in a single pass in the continuous process, whereas recirculation is required in the batch process. In the continous process, a fraction of the concentrate volume is rejected and replenished with desalinated diluate.

1.3 Our Partner: Eureka Forbes Ltd.

Our sponsor and collaborator, Eureka Forbes Ltd (EFL) has played an important role in providing safe drinking water to the Indian public. With the introduction of the original Aquaguard UV water purifier in 1984, the company mobilized a team to visit individual homes and demonstrate the benefits of water purification directly to customers. Today, Aquaguard continues to a be a trusted brand, and maintains a dominant share in an otherwise competitive market. Due to their capabilities as a large scale manufacturer and experience in marketing, distribution, and servicing, EFL serves as a valuable partner for the development of domestic water desalination and purification systems for Indian homes.

1.4 Outline of the Thesis

Paired with the necessary pre and post-filtration, batch ED is shown to be a more efficient alternative to RO for household desalination in Indian cities; however, further development is required to improve its affordability. Therefore, the primary objective of this thesis is to investigate the design of the proposed desalination system, which is comprised of the stack and pumps, in order to suggest configurations that are more cost-competitive with existing RO devices.

A combination of modeling, simulation, prototyping, and testing was used address this task, as highlighted by the thesis outline provided below. While the content presented here is specifically targeted at the household scale, it is anticipated that the insight derived from this work is equally applicable to design at larger scales.

Chapter 2 - System Modeling
A model that predicts the rate of mass transfer and pressure drop through the batch ED system, based on dimensional variables, flow properties, and applied voltage is presented. This model forms the basis of the proceeding design work.

Chapter 3 - Model Validation

The model presented in Chapter 2 was validated using a lab-scale ED stack, which is of similar scale to the system being investigated for household application. Experimental set-up and results are discussed in this chapter.

Chapter 4 - Cost-Optimization

Cost-optimal design configurations of the ED stack, and associated pump selection were investigated for varying product water concentration and production rate requirements using simulation.

Chapter 5 - Prototype Fabrication and Testing

An optimized design was selected for prototyping and tested against the targeted production specifications at the Global Engineering and Research (GEAR) Lab at the Massachusetts Institute of Technology (MIT) and EFL's facility in Bangalore. Experimental results and design improvements for future prototype iterations are presented here.

Chapter 2

System Modeling

Models used in the development of the household electrodialysis (ED) device are described in this chapter. In order to develop a cost-effective system, which includes the selection of pumps, models that captured the dependency of the mass-transport to the flow in the stack were required. There are several approaches to modeling ED spanning simple polynomial correlations [29], analytical derivations [30–32], to computational fluid dynamics (CFD) simulations [33]. Motivated by reducing the computational cost of evaluating designs, while maintaining fidelity over a broad range of configurations, analytical equations and semi-empirical models were favored in this work. The models below were implemented in an object-oriented framework in MATLAB [34], thereby providing a modular construction to facilitate future modification and improvement.

Following common practice, this work models desalination assuming a sodium-chloride solution. While production rates may vary for other ions, design insights obtained using this treatment are expected to remain relevant.

2.1 Mass Transport

Figure 2-1 represents the physical batch ED system being designed. In this sytem, two pumps recirculate the diluate and concentrate from their respective tanks through the ED stack. In order to predict the desalination performance of this system, with

respect to batch duration and energy consumption, a model that captured the mass or ion transfer from the diluate tank to the concentrate tank via the ED stack was required. A similar approach to Ortiz *et al.* [30] was implemented for this work, but more detailed descriptions of the mass transfer processes are also available in Strathmann [23] and Tanaka [35].

2.1.1 Mass Balance

The rate change of the concentration in the diluate and concentrate tanks is obtained from

$$\frac{dC^t_{\text{dil}}}{dt} = \frac{Q_{\text{dil}}}{\mathbb{V}_{\text{dil}}}(C^s_{\text{dil}} - C^t_{\text{dil}}), \text{ and} \tag{2.1}$$

$$\frac{dC^t_{\text{conc}}}{dt} = \frac{Q_{\text{conc}}}{\mathbb{V}_{\text{conc}}}(C^s_{\text{conc}} - C^t_{\text{conc}}), \tag{2.2}$$

where Q_{dil} and Q_{conc} [L/hr] are the recirculation flow-rates in the diluate and concentrate circuits. C^t_{dil} and C^t_{conc} [mol/L] are the concentrations in the diluate and concentrate tanks, respectively, while C^s_{dil} and C^s_{conc} [mol/L] are the concentrations in the stack. Lastly, the recovery ratio r of the process is governed by the relative volumes of water in the diluate and concentrate tanks, $\mathbb{V}_{\text{dil}}$ [L] and $\mathbb{V}_{\text{conc}}$ [L], such that

$$r = \frac{\mathbb{V}_{\text{dil}}}{\mathbb{V}_{\text{dil}} + \mathbb{V}_{\text{conc}}}. \tag{2.3}$$

In evaluating the recovery ratio, the volume of water in piping and within the ED stack is considered negligible with respect to the volume in the tanks. Water transport across the membranes during desalination due to osmosis and electro-osmosis is also neglected because the rate of transport due to these effects is on the order of 100 times smaller than the targeted production rate for this application (see Appendix A).

Mass balance within each channel of the ED stack accounts for advection, ion

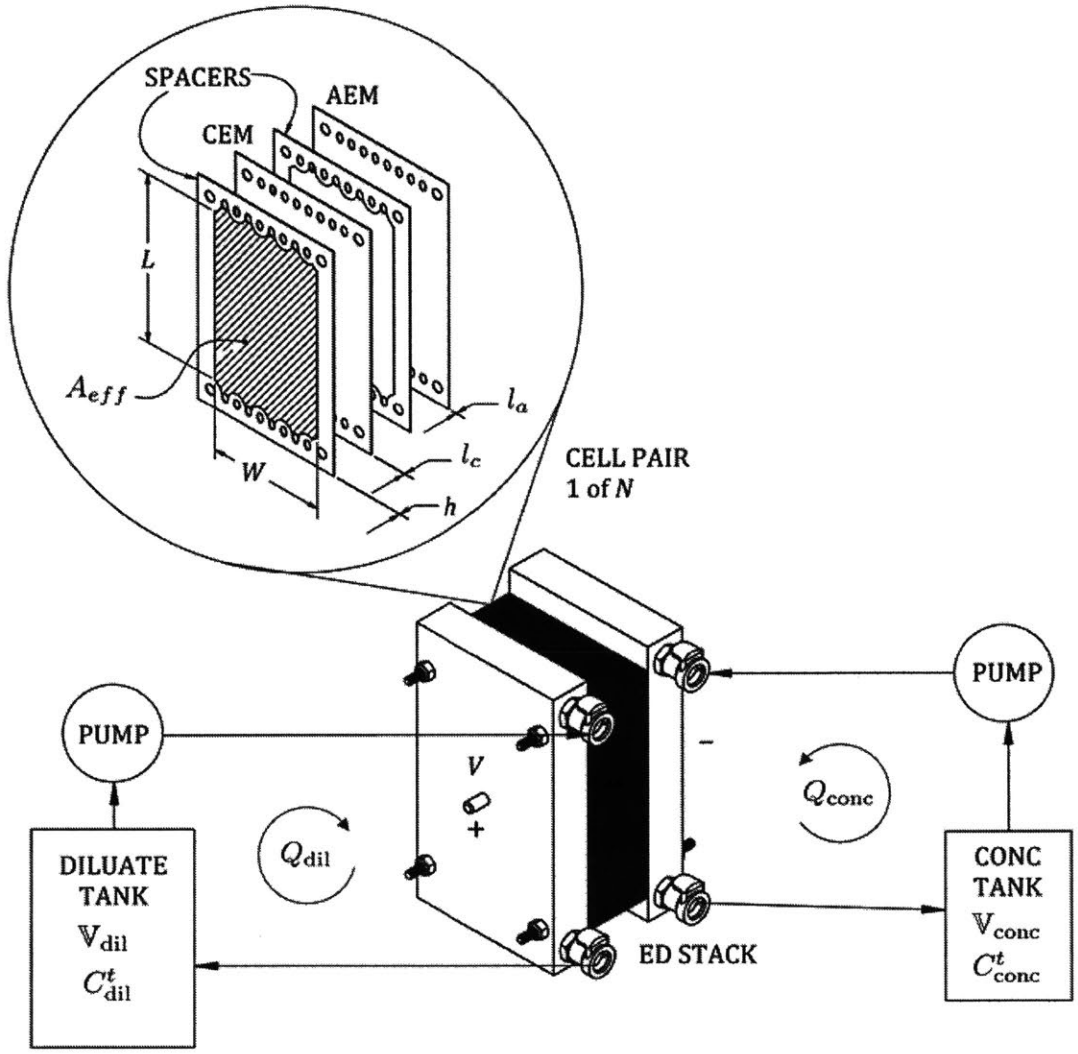

Figure 2-1: Schematic of a batch ED system, and an individual cell-pair, highlighting variables in mass transport equations. The pumps circulate the diluate and concentrate from the respective tanks through the ED stack. In the ED stack, each cell-pair is composed of two spacers, one each for the diluate and concentrate flows, separated by cation (CEM) and anion (AEM) exchange membranes.

migration due to the presence of an electric field, and back-diffusion across the membranes due to the concentration differences between the concentrate and diluate channels. Hence, the rate change of concentration in the diluate and concentrate channels is given by

$$\frac{dC^s_{\text{dil}}}{dt} = \frac{1}{N\mathbb{V}_c}[Q_{\text{dil}}(C^t_{\text{dil}} - C^s_{\text{dil}}) - \frac{N\phi I}{zF} + \frac{NA_{eff}D_a(C^{\text{AEM}}_{\text{conc}} - C^{\text{AEM}}_{\text{dil}})}{l_a} + \frac{NA_{eff}D_c(C^{\text{CEM}}_{\text{conc}} - C^{\text{CEM}}_{\text{dil}})}{l_c}], \text{ and} \tag{2.4}$$

$$\frac{dC^s_{\text{conc}}}{dt} = \frac{1}{N\mathbb{V}_c}[Q_{\text{conc}}(C^t_{\text{conc}} - C^s_{\text{conc}}) + \frac{N\phi I}{zF} - \frac{NA_{eff}D_a(C^{\text{AEM}}_{\text{conc}} - C^{\text{AEM}}_{\text{dil}})}{l_a} - \frac{NA_{eff}D_c(C^{\text{CEM}}_{\text{conc}} - C^{\text{CEM}}_{\text{dil}})}{l_c}], \tag{2.5}$$

respectively, where subscripts a and c denote the anion (AEM) and cation (CEM) exchange membranes. N is the number of cell-pairs, ϕ is the current efficiency, z is the ion charge, F is Faraday's constant, l is the thickness of the ion exchange membrane, D is its diffusivity, and $C^{\text{CEM}}_{\text{dil}}$, $C^{\text{AEM}}_{\text{dil}}$, $C^{\text{CEM}}_{\text{conc}}$, and $C^{\text{AEM}}_{\text{conc}}$ are the concentrations of the diluate and concentrate streams at the interfaces with the AEMs and CEMs. Ion transport occurs over an effective area A_{eff}, given by

$$A_{eff} = \eta LW. \tag{2.6}$$

Note that the effective area available for ion transport A_{eff} is lower than the product of the length L and width W of the cell-pair due to the presence of a spacer whose open-area porosity is η (Eqn. 2.37). Similarly, the volume of the channel V_c [m^3] is also modified due to the presence of a spacer, according to

$$V_c = \varepsilon LWh, \tag{2.7}$$

where ε is the fraction of the total volume that is not occupied by the spacer (Eqn. 2.40). In order to model the ion migration, represented by current I [A], we narrow

our focus to an individual cell-pair in the following section.

2.1.2 Current Density

An analogous circuit (Fig.2-2) is used to facilitate a discussion of the terms affecting ion movement from the diluate to the concentrate channels, which is represented a current density i [A/m^2] whereby

$$i = \frac{I}{A_{eff}}. \tag{2.8}$$

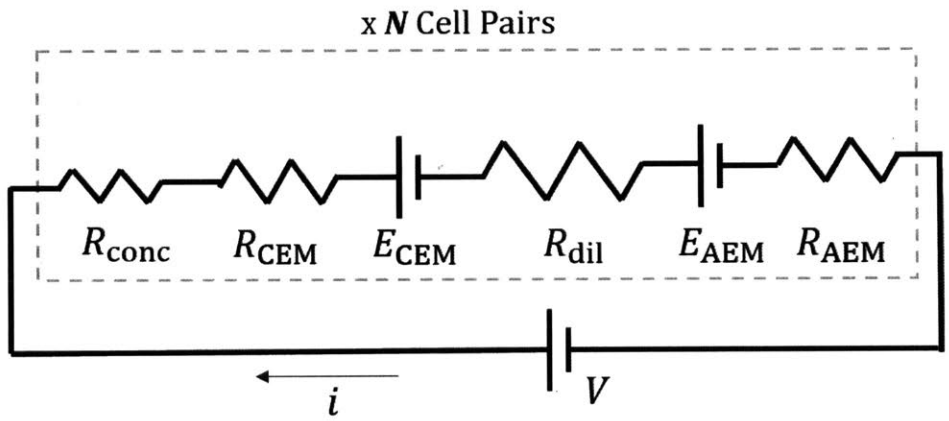

Figure 2-2: The ED stack is represented by an analogous circuit whereby ion transport is modeled by a current i due to the application of a voltage V over N cell-pairs. Exchange membranes (AEM and CEM) and channels (diluate and concentrate) are modeled using effective resistances R and back-potentials E.

An applied voltage V [V] drives the movement of ions through a series of diluate and concentrate channels separated by alternating cation (CEM) and anion (AEM) exchange membranes with static resistances R_{CEM} and R_{AEM} [Ω-m^2], respectively. Therefore,

$$i = \frac{V/N - E_{\mathrm{CEM}} - E_{\mathrm{AEM}}}{R_{\mathrm{conc}} + R_{\mathrm{dil}} + R_{\mathrm{CEM}} + R_{\mathrm{AEM}}}, \tag{2.9}$$

where other ohmic resistance terms are associated with the diluate and concentrate streams (R_{dil} and R_{conc}). They increase with solution resistivity ρ_s [Ω-m] and channel

height h [m] as per

$$R = \rho_s h. \tag{2.10}$$

Finally, a back-potential develops across the membranes due to salinity differences in alternating channels and concentration polarization (Fig.2-3). These terms (E_{CEM} and E_{AEM}) [V] are each modeled as

$$E_{\text{mem}} = \frac{RT}{F} \ln\left(\frac{a_{\text{conc}}^{\text{wall}}}{a_{\text{dil}}^{\text{wall}}}\right) \tag{2.11}$$

assuming perfect ion-selective membranes, where R is the gas constant (J/mol-K), T [K] is the temperature of the solution, and the activities $a_{\text{dil}}^{\text{wall}}$ and $a_{\text{conc}}^{\text{wall}}$ are related to the wall (or interface) concentrations, $C_{\text{dil}}^{\text{CEM}}$, $C_{\text{dil}}^{\text{AEM}}$, $C_{\text{conc}}^{\text{CEM}}$, and $C_{\text{conc}}^{\text{AEM}}$.

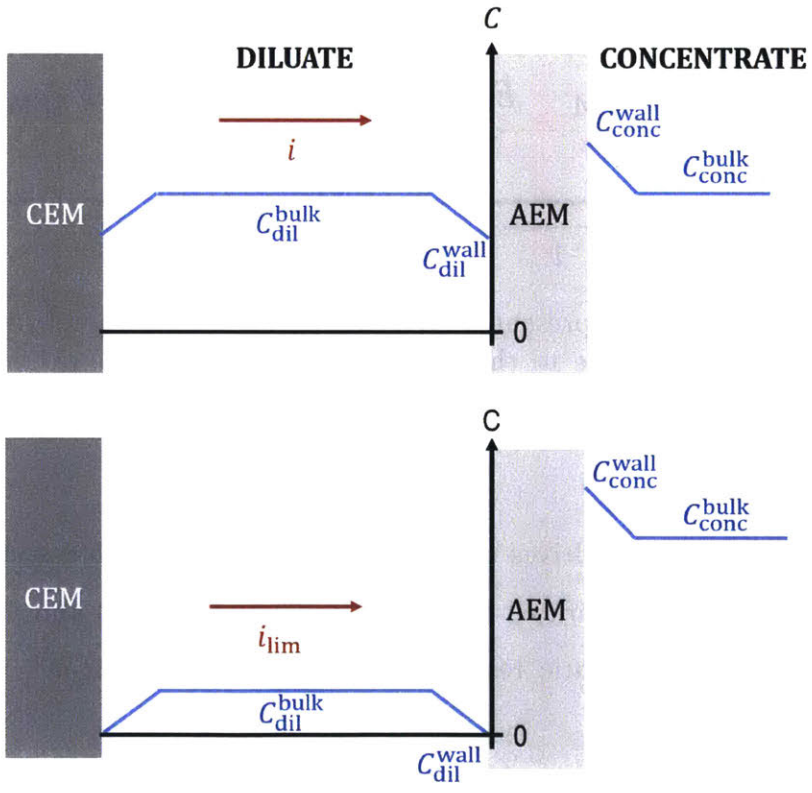

Figure 2-3: Ion transfer number differences in the bulk solution and membrane produces a polarization effect, hence the concentration at the wall C^{wall} differs from the bulk C^{bulk} under an applied current density i (top). The limiting current density i_{lim} produces a zero C_{dil}^{wall}, and is a function of C_{dil}^{bulk} (bottom).

The concentrations at the walls are in-turn affected by the current density, since a greater i will produce a greater depletion of the ions at the diluate-membrane interfaces. By balancing the migration of ions across either the CEM or AEM with the diffusion of ions to the corresponding interface, expressions of the form

$$C_{\text{dil}}^{\text{AEM}} = C_{\text{dil}}^{s} - \frac{\phi i}{zFk}(T_{\text{AEM}} - t_a), \text{ and} \tag{2.12}$$

$$C_{\text{conc}}^{\text{CEM}} = C_{\text{conc}}^{s} + \frac{\phi i}{zFk}(T_{\text{CEM}} - t_c), \tag{2.13}$$

are obtained to estimate the interface concentrations, where t_c and t_a represent the cation and anion transport numbers in the bulk solution, respectively. The transport numbers for the membranes T is typically set to 1 under the assumption of perfect ion selectivity.

The dominant impedance in brackish water desalination using ED is the resistance of the diluate channels because the resistivity increases sharply at low concentrations (Fig.2-4). In addition, the high membrane potential and low limiting current are expected to drastically increase the cost of designs targeted at achieving the lowest product water concentrations.

2.1.3 Limiting Current Density

A concentration boundary layer evolves at the interface between the fluid in the channels and the membranes when a voltage is applied. As a result, the maximum rate of ion transport is bounded by a current density which produces a zero ion concentration at the membrane interface in the diluate channel (Fig.2-3). This limiting current density i_{lim} [A/m^2], which plays an important role in the design of an ED stack for brackish water desalination, is estimated using

$$i_{lim} = \frac{C_{dil}^{s} zFk}{T_{\text{mem}} - t}, \tag{2.14}$$

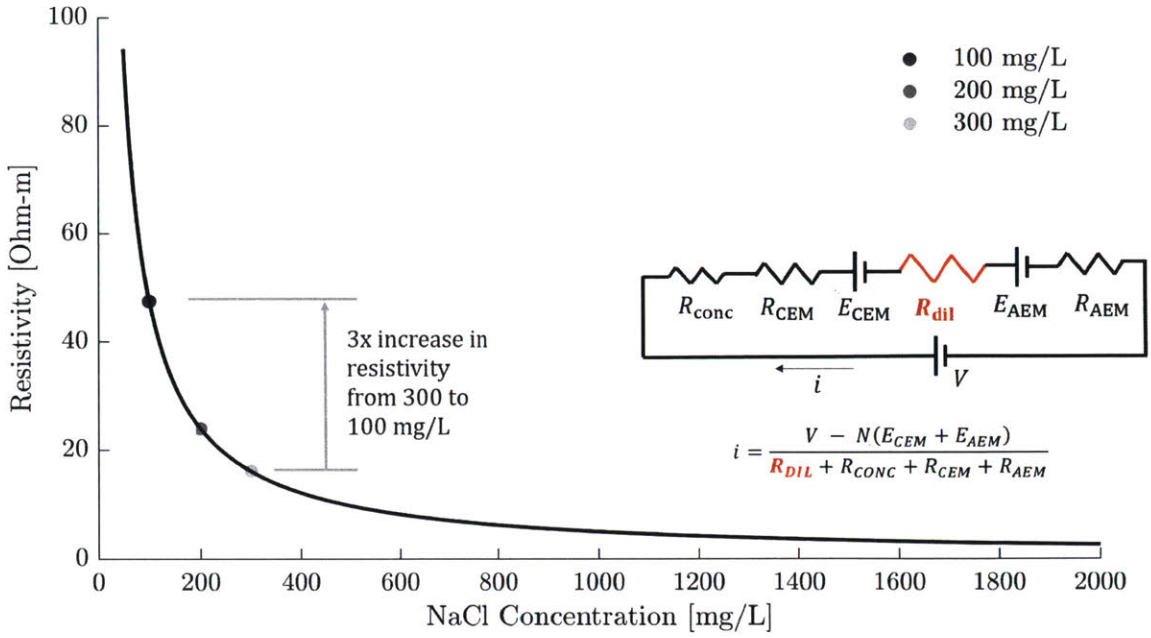

Figure 2-4: Resistivity of a NaCl solution modeled using Faalkenhaagen equation [36]. As shown, the resistivity increases sharply at low concentrations.

where T_{mem} is the transport number of the counter-ion in the membrane, and t is the transport number of the same ion in the bulk solution where its concentration is C^s_{dil}.

The model used in this work deviates from Ortiz *et al.* in the treatment of the boundary-layer mass transfer coefficient k [m/s]. Rather than being a constant, it is treated as being dependent on hydrodynamic factors such as the flow-velocity, which in-turn is affected by the geometry of the ED stack and the choice of pump.

2.1.4 Coupling Mass Transport to Flow

By definition, the Sherwood Number Sh is related to k by

$$k = \frac{ShD}{d_h}. \tag{2.15}$$

D is the diffusion coefficient of the solution, and the hydraulic diameter d_h defined by Pawlowski (et al.) [37] is

$$d_h = \frac{4\varepsilon}{2/h + (1-\varepsilon)(8/h)}. \tag{2.16}$$

The mass transfer is then correlated to the flow properties via

$$Sh = 0.29 Re_d^{0.5} Sc^{0.33} \text{ [37]}, \tag{2.17}$$

where the Schmidt Number Sc is a material-dependent, non-dimensional quantity, and the Reynolds Number Re_d which characterizes the flow is defined as

$$Re_d = \frac{\rho u_{ch} d_h}{\mu}, \tag{2.18}$$

where ρ [kg/m^3] is the density of the solution, μ [Pa-s] is the viscosity of the solution, and the velocity in the spacer-filled channel u_{ch} is calculated using Eqn.2.39.

From Equations 2.14-2.18, it is evident that a high linear flow velocity in the channels will produce an increase in the mass transfer coefficient and a corresponding increase in the limiting current density. Using optimization, we sought to balance these benefits against costs associated with larger pressure drops caused by increased flow velocity.

2.2 Pressure Drop

A similar approach to Pawlowski *et al.* [37], with correlations derived from Ponzio *et al.* [38], was used to predict the pressure drop for each configuration of the ED system being investigated. Minor loss coefficients for dividing and converging flows were obtained from Hager [39].

Each contributor to the total pressure drop in the identical diluate or concentrate circuits within the ED stack (Figure 2-5) can be represented by an analogous resistance network (Fig. 2-6). Individual loss terms are detailed in 2.2.1 through 2.2.6; but the dominant term is associated with the flow through the channels for small-sized stacks (Fig.2-7). This result agrees with the experimental findings of Pawlowski *et al.* [37], and is a necessary for achieving even flow across the cell-pairs.

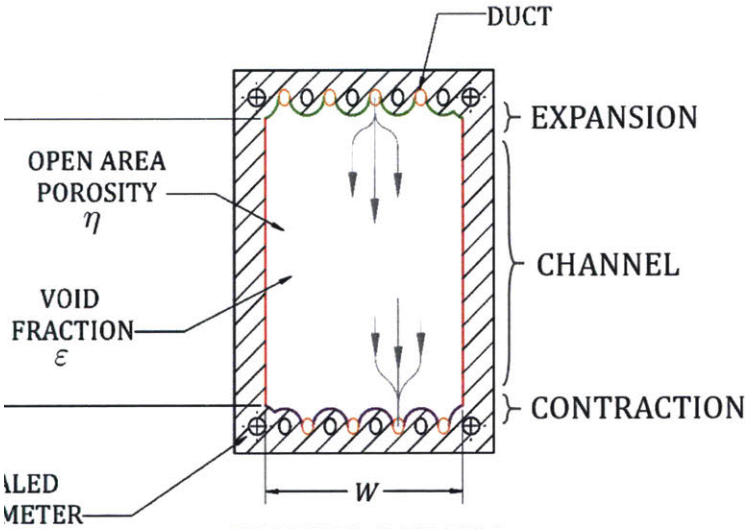

CHANNEL DETAILS

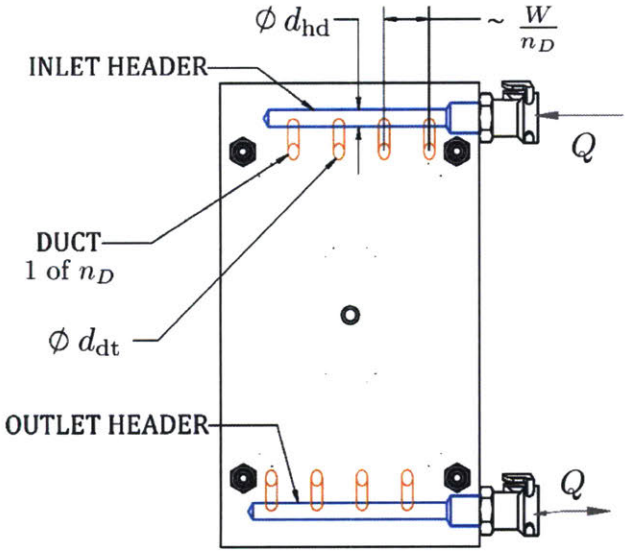

END PLATE DETAILS

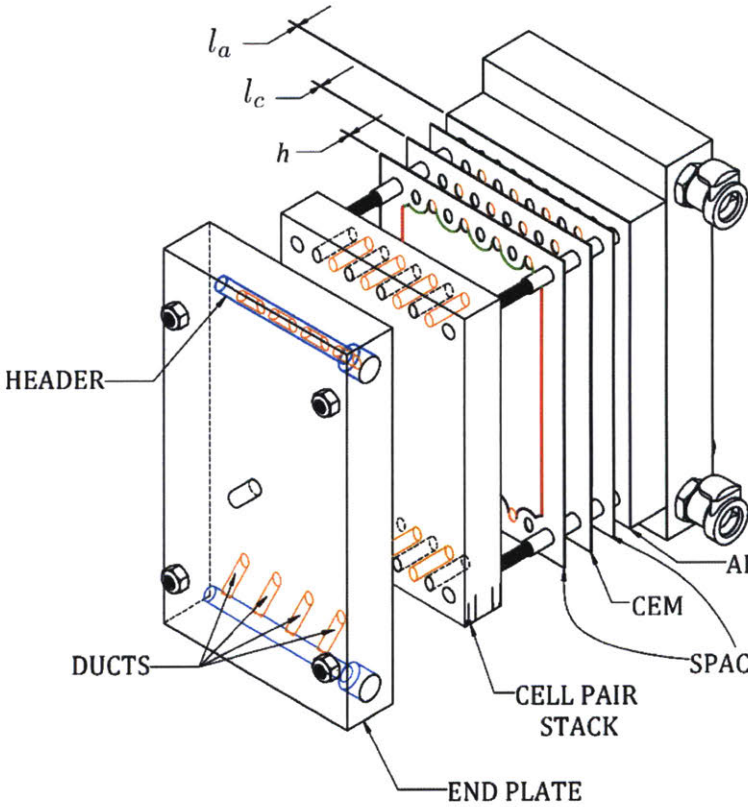

LEGEND:

HEADER — CHANNEL

DUCT — CONTRACT

EXPANSION

e 2-5: Flow circuit (either concentrate or diluate) through the ED stack, highlighting key variables that affect pr

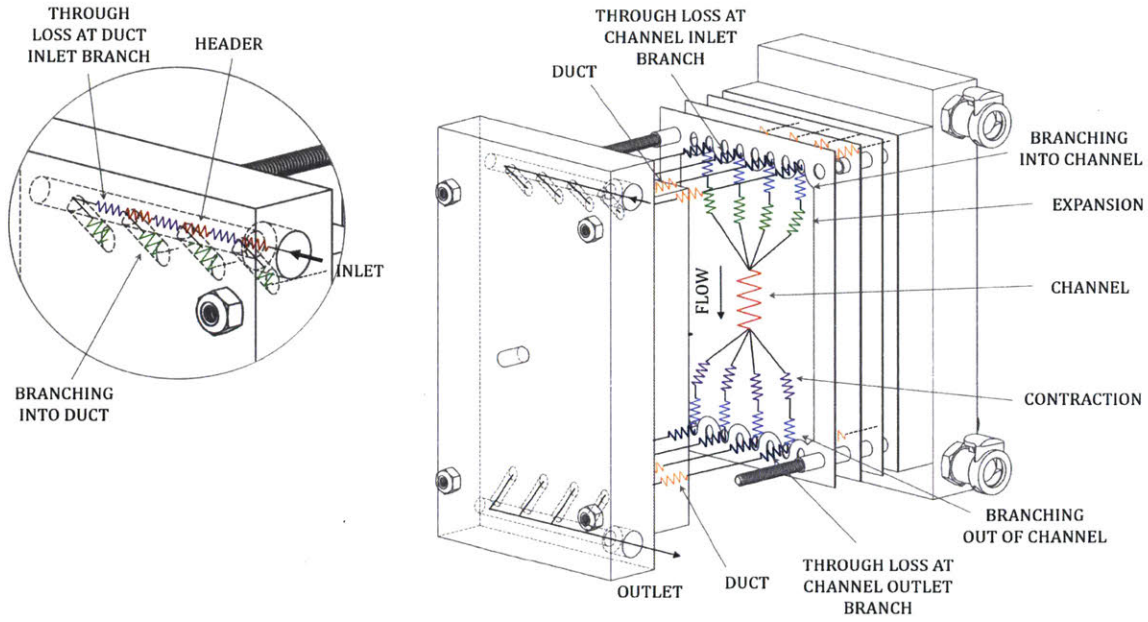

Figure 2-6: Analogous resistor network depicting sources of pressure drop in the diluate, or identical concentrate, circuit.

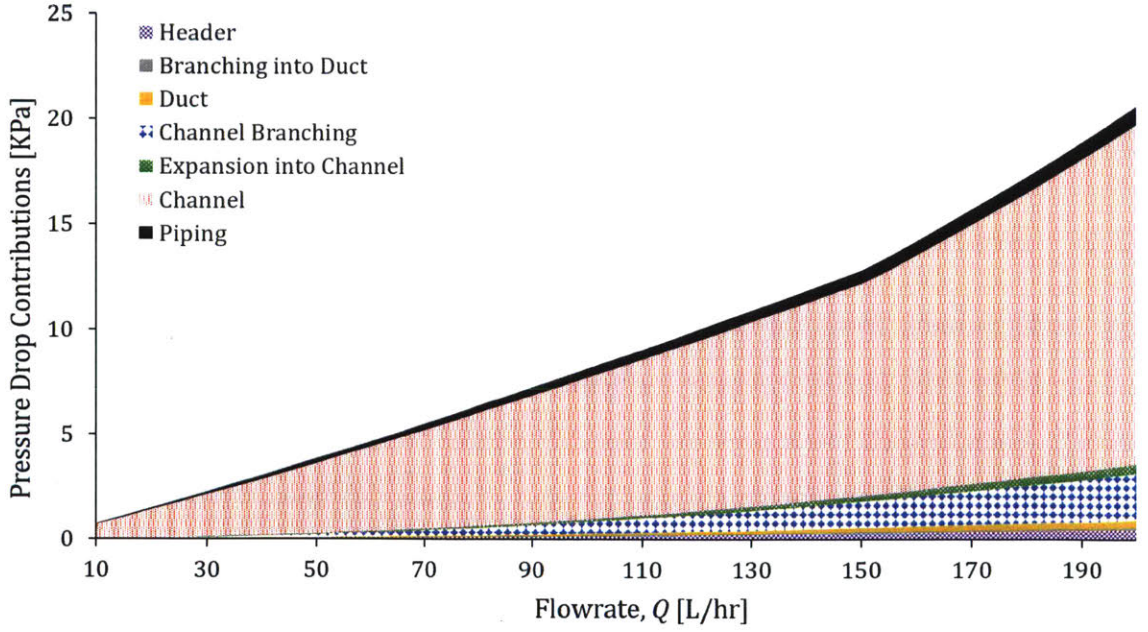

Figure 2-7: Pressure drop in each element of the flow circuit, modeled for the 18 cell pair, 8 cm x 8 cm, ED stack used by Nayar *et al.* [27]. The channel provides the dominant resistance to flow.

2.2.1 Header

The header is situated in the housing and distributes the flow to the ducts. The volumetric flow-rate decreases along the length of the header as flow is distributed to the ducts. The volumetric flow-rate in the header Q_h before duct j of total ducts n_D is

$$Q_h = Q(1 - \frac{j-1}{n_D}). \tag{2.19}$$

The corresponding velocity in the header u_{hd} is

$$u_{hd} = \frac{4Q_h}{\pi d_{hd}^2}, \tag{2.20}$$

where d_{hd} is the header diameter. The pressure drop contribution from flow through each section of the header (separated by ducts) is calculated using the Hagen-Poiseuille equation, given as

$$\Delta P_h = \frac{128\mu Q_h W}{\pi d_{hd}^4 n_D}, \tag{2.21}$$

where W/n_D approximates the length of the section.

2.2.2 Branching into, and from Ducts

Flow paths branch from the header to the ducts at the inlet of each circuit, and combine before the outlet, thereby inducing a pressure loss at both ends of the flow network. Each branch has a pressure loss ΔP related to through-flow (t) and branch-flow (d), and is different for combining (c) and dividing (d) flows. These terms were modeled by the Darcy-Weisbach equation

$$\Delta P = \frac{1}{2} K \rho u_{\mathrm{hd}}^2, \tag{2.22}$$

where the minor loss coefficients K are summarized in Table 2.1.

The area ratio r_A and volumetric flow ratio r_Q required for calculating the loss

Table 2.1: Loss Coefficients for Branching Ducts from Header Flow [39]

Pressure Loss Term	**Loss Coefficient,** K
$\Delta P_{t,d}$	$\frac{4}{5}r_Q(r_Q - 0.5)$
$\Delta P_{t,c}$	$r_Q(2 - r_A)$
$\Delta P_{b,d}$	$1 - 2r_Q\cos(\frac{3\pi}{8}) + r_Q^2$
$\Delta P_{b,c}$	$-1 + 4r_Q + (\frac{1}{r_A^2} - 2)r_Q^2$

coefficient are

$$r_A = \frac{d_{\text{dt}}}{d_{\text{hd}}}, \text{ and}$$
$$r_Q = \frac{1}{n_D - j + 1}, \tag{2.23}$$

where d_{dt} is the diameter of each duct. Since the ducts provide parallel flow from the header to the channel (Fig.2-6), all losses pertaining to the header and associated branching were calculated for the representative first duct, $j = 1$.

2.2.3 Ducts

The pressure loss contribution from the ducts is modeled similarly as the headers. Assuming that the total volumetric flow is equally divided among the N cell-pairs, the volumetric flow-rate through the duct after each cell-pair k is

$$Q_{\text{dt}} = \frac{Q}{n_D}(1 - \frac{k-1}{N}). \tag{2.24}$$

Therefore, the associated velocity u_{dt} and pressure drop ΔP_{dt} between cell-pairs $k-1$ and k are

$$u_{\text{dt}} = \frac{4Q_{\text{dt}}}{\pi d_{\text{dt}}^2}, \text{ and} \tag{2.25}$$

$$\Delta P_{\text{dt}} = \frac{128\mu h Q_{\text{dt}}}{\pi d_{\text{dt}}^4} \tag{2.26}$$

2.2.4 Branching into, and from Channels

The pressure drop associated with the branching of flow from and to the channels was also modeled using the Darcy-Weisbach equation, but with respect to the velocity in the duct u_{dt}, so that

$$\Delta P = \frac{1}{2} K \rho u_{\mathrm{dt}}^2, \tag{2.27}$$

with a different set of minor loss coefficients K which assume that the cross-sectional area of the branch diverting flow into the channel is small compared to that of the duct (Table 2.2).

Table 2.2: Loss Coefficients for Branching Channels from Duct Flow [39]

Pressure Loss Term	**Loss Coefficient, K**
$\Delta P_{t,d}$	$(1+r_u)(1-r_u)^2$
$\Delta P_{t,c}$	$r_Q(2-r_Q)$
$\Delta P_{b,d}$	1
$\Delta P_{b,c}$	$-1+4r_Q+(\frac{1}{r_A^2}-2)r_Q^2$

The ratio of the flow-rate entering the channel and the flow-rate in the preceding segment of the duct r_Q is approximated using

$$r_Q = \frac{1}{N-k+1}, \tag{2.28}$$

whereas the ratio of the flow velocity in the duct after the channel to that before it is

$$r_u = \frac{N-j}{N-k+1}. \tag{2.29}$$

Since the channels are arranged to provide parallel flow, pressure loss from the duct and through branching is calculated for the representative first cell-pair, $k = 1$.

Lastly the entry from the duct to the channels is non-circular. Hence, the area-ratio r_A, where

$$r_A = \frac{d_{\mathrm{c,hy}}}{d_{\mathrm{dt}}}, \tag{2.30}$$

is calculated using a hydraulic diameter

$$d_{\mathrm{c,hy}} = 4\frac{\frac{1}{2}\pi d_{\mathrm{dt}} h\varepsilon}{\pi d_{\mathrm{dt}} + 2h}, \tag{2.31}$$

where ε is the spacer void fraction (Eqn.2.40).

2.2.5 Expansion and Contraction of Channels

Fluid flow that enters the channel through the duct suddenly expands to occupy the full width of the channel while slowing down in the process. The pressure drop associated with this loss in kinetic energy can be expressed using the Borda-Carnot equation,

$$\Delta P_{ex} = \frac{1}{2}\rho u_{ch}^2 (\frac{\varepsilon W}{d_{\mathrm{dt}}} - 1)^2, \tag{2.32}$$

where u_{ch} is the flow velocity in the channel (2.39). In contrast, the fluid increases in speed at the channel exit, converting the pressure into kinetic energy. Here, the associated pressure-loss is considered negligible [37].

2.2.6 Channels

Pressure loss in the channels is modeled as

$$\Delta P_{ch} = C_p \rho f \frac{L}{h} u_v^2, \tag{2.33}$$

where C_p=0.75 is an empirical coefficient, L [cm] is the length of the channel's active area, and the void channel (without spacer) velocity u_v [cm/s] is related to the volumetric flow in each circuit Q [L/hr] by

$$u_v = \frac{Q}{WhN}, \tag{2.34}$$

where W [cm] is the width of the active area and N is the number of cell-pairs. Then, using an alternative Reynolds Number Re definition of

$$\mathrm{Re} = 2\frac{\rho u_v h}{\mu}, \tag{2.35}$$

the friction factor f is approximated from the results of Ponzio *et al.* [38] using the correlations

$$\begin{aligned} f &= 1500/\mathrm{Re} \text{ for } \mathrm{Re} < 58, \text{and} \\ f &= 116/\mathrm{Re}^{0.37} \text{ for } \mathrm{Re} \geq 58. \end{aligned} \tag{2.36}$$

The friction factor correlations were obtained using CFD simulation of woven spacers with a spacing-to-diameter ratio of 1.5. The geometry of spacers that are implemented in the physical device may deviate from this ratio; however, it is anticipated that the corresponding pressure drop predictions will still be sufficiently accurate for pump sizing.

2.3 Flow Spacer

In addition to inducing a greater pressure drop, a thinner spacer will also provide a lower area for ion transport because its filaments tend to be more closely woven. This effect is characterized by adjusting the area by a porosity value η or 'shadow factor', calculated as

$$\eta = \frac{(l_f - d_f)^2}{(l_f)^2}, \tag{2.37}$$

assuming an orthogonal arrangement of filaments (Fig.2-8).

The spacing l_f and the diameter d_f of filaments are related to the height of each channel (spacer thickness) by

$$\begin{aligned} l_f &= 1.5h, \text{ and} \\ d_f &= \frac{h}{2cf} \end{aligned} \tag{2.38}$$

using a compaction factor cf of 0.946 [40]. A conservative factor of 1.5 in Eqn.2.38

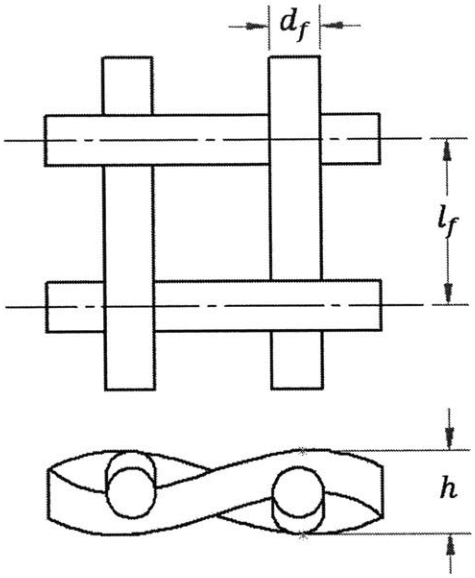

Figure 2-8: Detail view of woven mesh which is often used as a spacer and turbulence promoter in flow channels.

was applied after surveying the product offerings from manufacturers of woven meshes [41, 42]. Note that this is a smaller length-to-diameter ratio than that associated with the friction factor correlations (Eqn.2.36); however, it provides a more conservative estimate of the required area for a desired rate of ion transport. Due to the presence of a flow-spacer, the actual linear flow velocity u_{ch} in the spacer is approximated from the void channel flow velocity (Eqn.2.34) using

$$u_{ch} = \frac{u_v}{\varepsilon}, \tag{2.39}$$

where the void fraction ε is defined as the volume of the channel that is not occupied by the spacer, given by

$$\varepsilon = 1 - \frac{\pi d_f^2}{2 l_f h}. \tag{2.40}$$

2.4 Model Summary and Future Improvements

A model that predicts the rate of desalination and pressure drop for a batch ED system, given its dimensional, voltage, and flow parameters, is described in this chapter. Most importantly, it relates the flow through a channel and the mass transport capacity across the bounding ion exchange membranes. This level of detail is necessary when designing an ED system for household use because the velocity obtained in the channels is associated with the pumps that are implemented, and the cost of these pumps is a non-negligible fraction of the total system cost. While this model is sufficiently detailed for the optimization and design work presented in this thesis, the following improvements will further increase accuracy and design freedom:

- Accurate prediction of the pressure drop and mass transfer requires consideration of several other variables including the spacer orientation, spacing and angle between filaments, and whether they are woven or not. This level of detail was not deemed necessary for this analysis, but several studies have aimed to characterize these relationships [40, 43–46]. Their results could be implemented for more detailed design deliberation in the future.

- The existing model treats the membranes as having a static electrical resistance, but some studies suggest that the resistance changes as a function of the wetting solution's concentration [47]. It may be important to implement this relationship in the model to improve desalination rate predictions.

- Future iterations of the model should also consider the reduction-oxidation reactions occurring at the electrodes and their effect on the current efficiency.

Chapter 3

Model Validation

The models described in Chapter 2 were validated by performing a series of experiments on a lab-scale ED test stack. The objective of this exercise was to assess the accuracy of the models before implementing them in designing the household system. These experiments were performed at the GEAR Lab using the set-up outlined in Figure 3-1. The test apparatus consisted of a PC*Cell* 64 0 02 lab-scale ED test unit [48] outfitted with cell-pairs, each with an active area that measured 8 cm x 8 cm. Relevant stack and membrane parameters that were used in simulation are provided in Table 3.1.

Table 3.1: PC*Cell* 64 0 02 Lab-Scale ED Stack Details

Parameter	**Value**	**Reference**
Length of Active Area	8 cm	[48]
Width of Active Area	8 cm	[48]
Channel Thickness	0.35 mm	[48]
Spacer Area Porosity	0.62	Measured
Number of Cell-Pairs	14	-
CEM (PC-SK) Resistance	2.5 Ω-cm	[49]
CEM (PC-SK) Thickness	200 μm	[49]
AEM (PC-SA) Resistance	1.8 Ω-cm	[49]
AEM (PC-SA) Thickness	200 μm	[49]
Membrane Diffusion Coefficients	3.28 x 10^{-11} [m^2/s]	[30]

In all the tests, deionized water was mixed with lab-grade sodium chloride to obtain the desired salinity. The solution was held within a single beaker (for limiting

current density tests), or divided into two beakers at the desired recovery ratio (for desalination tests). During the experiment, magnetic stirring plates were used within the beakers to mix the diluate and concentrate solutions, and a Model 3250 meter (Jenco Instruments) was used to monitor diluate and concentrate conductivity. Two NF300 KPDC diaphragm pumps (KNF Flodos) were used to circulate the diluate and concentrate from the tank and through the stack. The flow rate through the stack was varied using 7430 Series glass tube flowmeters with valves (King Instrument), and pressure dial-gauges were installed to monitor pressure upstream and downstream of the stack in the diluate and concentrate streams.

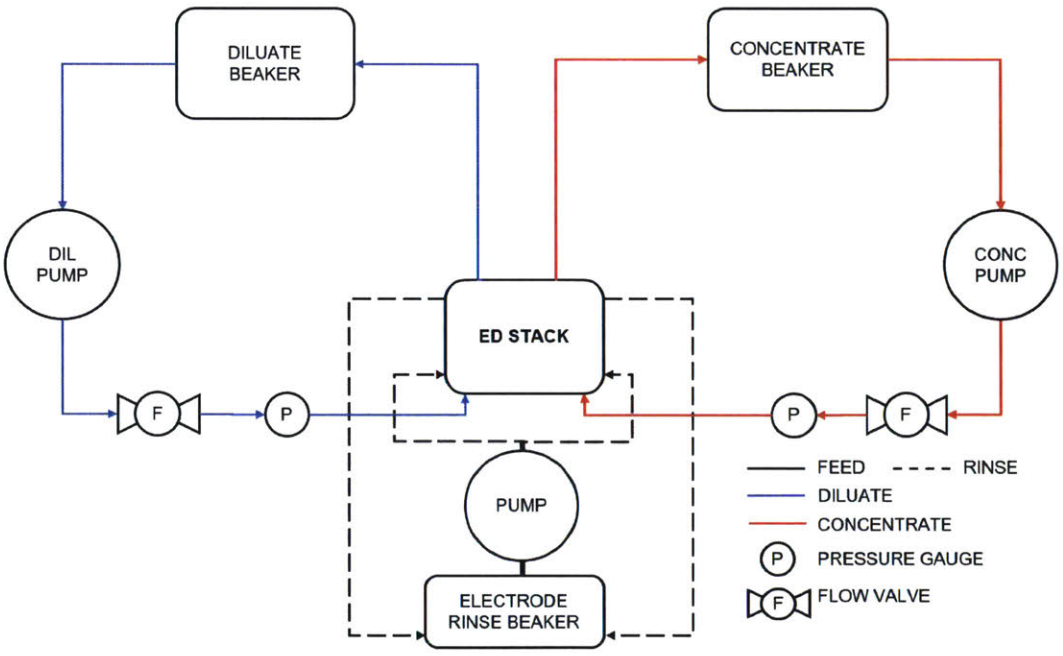

Figure 3-1: Schematic of lab-scale experimental set-up at the GEAR Lab.

A separate solution of deionized water and sodium sulfate (0.2 M) was formulated for the electrode rinse stream. It was circulated during each test by an MD-20RZ centrifugal pump (Iwaki) at approximately 2.5 LPM.

3.1 Limiting Current Density

The limiting current density is the maximum current density that can be applied across the ED stack before the splitting of water molecules, into hydrogen and hydroxide ions, occurs in the diluate channels. In order to minimize the membrane area, and corresponding cost, of the proposed batch ED system, it is necessary to predict this maximum current density as a function of the stack geometry, solution concentration, and flow-rates.

The limiting current was measured based on a common procedure, which has been outlined previously in literature [23, 50, 51]. For each test, the current was measured at voltages of 0 through a maximum of 100 V in increments of 4 V, while circulating a solution of constant concentration from a single beaker, through both the diluate and concentrate circuits, at a fixed flow-rate. As indicated in the test outline presented in Table 3.2, the same procedure was then repeated at different concentrations and flow-rates.

Table 3.2: Limiting Current Density Tests on Lab-Scale Test Stack

Tests	**Concentration [mg/L]**	**Flow-Rates [L/hr]**
1-3	250	
4-6	500	
7-9	1000	
10-12	1500	30, 60, 90
13-15	2000	
16-18	2500	
19-21	3000	

For each test, the measured current was plotted against the voltage. The data can be divided into two regions which are differentiated by the slope of the current-voltage relationship (Fig. 3-2): under-limiting current and over-limiting current. The two slopes intersect at the limiting current.

The limiting current I_{lim} was divided by the effective area (Eqn. 2.6) to obtain the limiting current density i_{lim}. It was found that i_{lim} varied with both the concentration of the solution and the flow-rates (Fig.3-3); hence the selection of pumps and design of the flow paths are an important consideration in the design of the ED system.

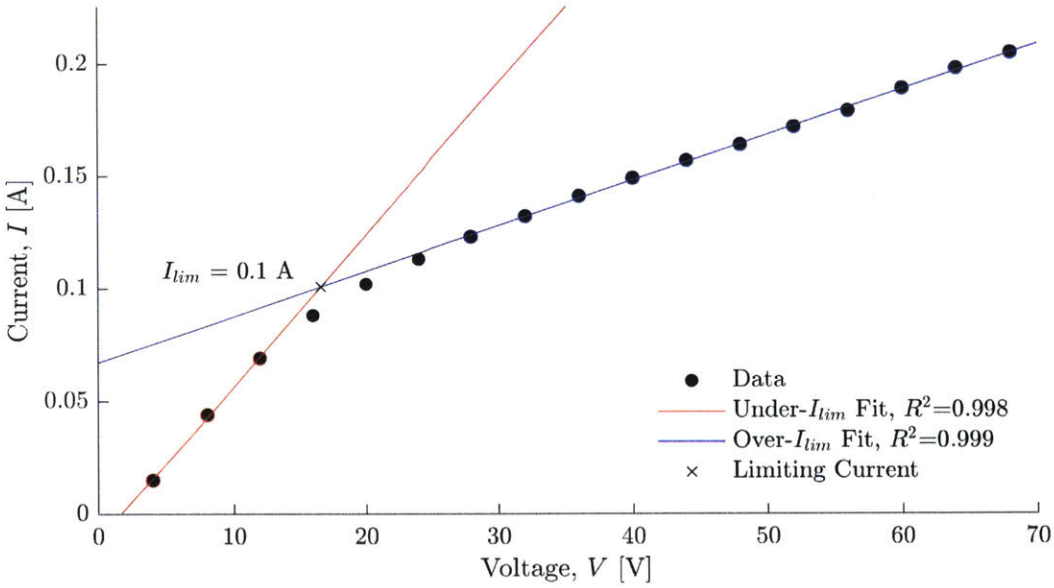

Figure 3-2: Measured current I plotted against applied voltage V for 250 mg/L solution circulated at 30 L/hr. The red and blue lines are linear fits of two distinct operating regions: under-limiting current, and over-limiting current. The intersection of the two lines occurs at the limiting current I_{lim}.

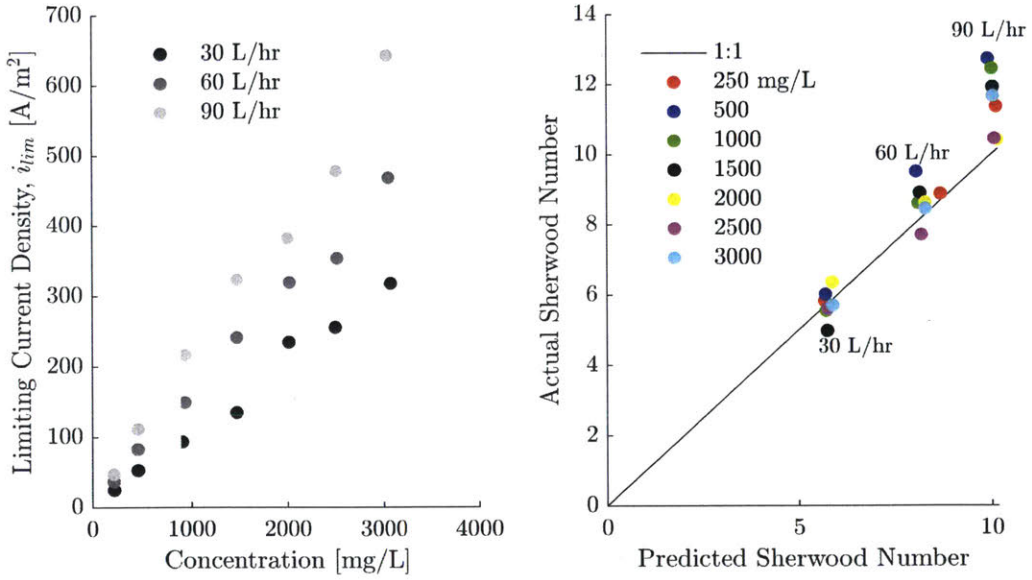

Figure 3-3: The limiting current density i_{lim} is plotted against the solution concentration for varying flow-rates, measured using the lab-scale PCCell 64002 ED test stack (*left*). Model-predicted Sherwood Numbers Sh closely matched the experimental values (*right*).

In order to compare the experimental results to the theoretical predictions derived using the model provided in Section 2.1.3, the results are also represented in terms of the non-dimensional Sherwood number Sh. As seen in Figure 3-3, the experimental results match closely with the theoretical predictions, thereby indicating that the models described in Chapter 2 are accurate.

3.2 Desalination

Desalination tests were also performed using the lab-scale experimental set-up to validate the full mass-transfer model which was presented in Section 2.1. A sodium-chloride solution was desalinated from a concentration of 3000 mg/L to 100-300 mg/L product water at varying recovery ratios and stack flow-rates (Table 3.3), with each test performed twice.

Table 3.3: Desalination Tests on Lab-Scale Test Stack

	Test 1	**Test 2**	**Test 3**
Applied Voltage [V]	8	10	11
Stack Flow-Rate [L/hr]	40	80	70
Feed Concentration [mg/L]	3000	3000	3000
Product Concentration [mg/L]	300	200	100
Concentrate Tank Volume [L]	1	1	0.4
Diluate Tank Volume [L]	1	1	1.6
Resultant Recovery Ratio	0.5	0.5	0.8

Figures 3-4 through 3-6 (*left*) compare the predicted and measured conductivity (dependent on concentration) trajectories. These results indicate that even though the actual rate of desalination was 5-27% higher than predicted, there was good agreement between the experiment and model.

By investigating the current against diluate conductivity in Figures 3-4 and 3-5 (*right*), it is evident that the current is predicted accurately for diluate conductivity lower than 2000 uS/cm, observed for approximately half of the batch duration, but is under-predicted at higher conductivity. It is likely that the modeled membrane resistance, which was provided by the manufacturer, is higher than the actual value. This inconsistency would explain the higher measured current at the start of the

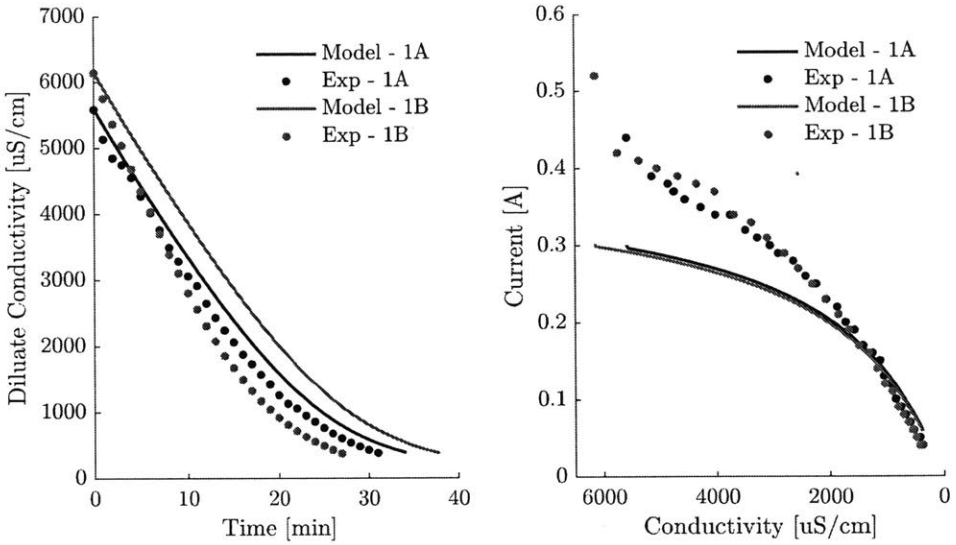

Figure 3-4: Model and experimental diluate conductivity vs time (*left*) and current vs diluate conductivity (*right*) for Test 1. A 3000 mg/L solution was desalinated to 300 mg/L at 50% recovery.

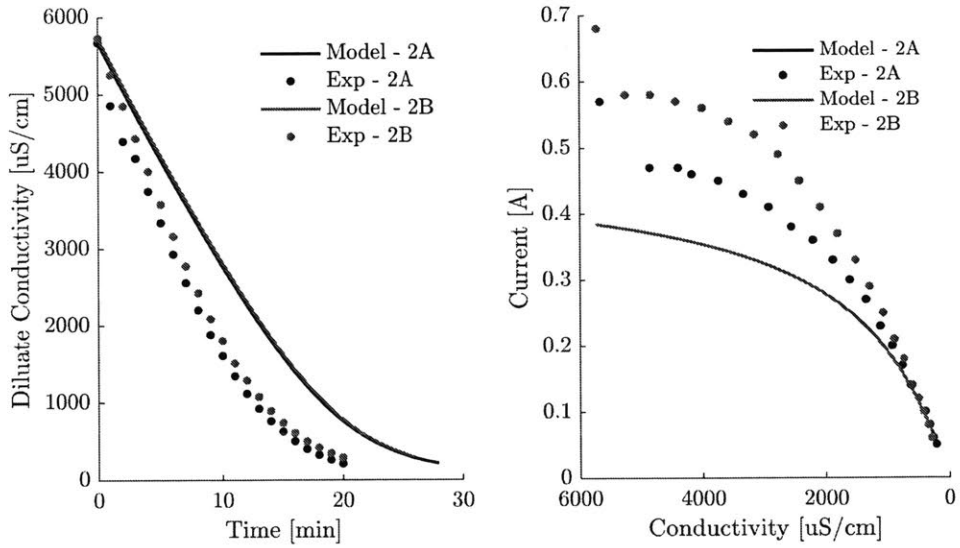

Figure 3-5: Model and experimental diluate conductivity vs time (*left*) and current vs diluate conductivity (*right*) for Test 2. A 3000 mg/L solution was desalinated to 100 mg/L at 50% recovery.

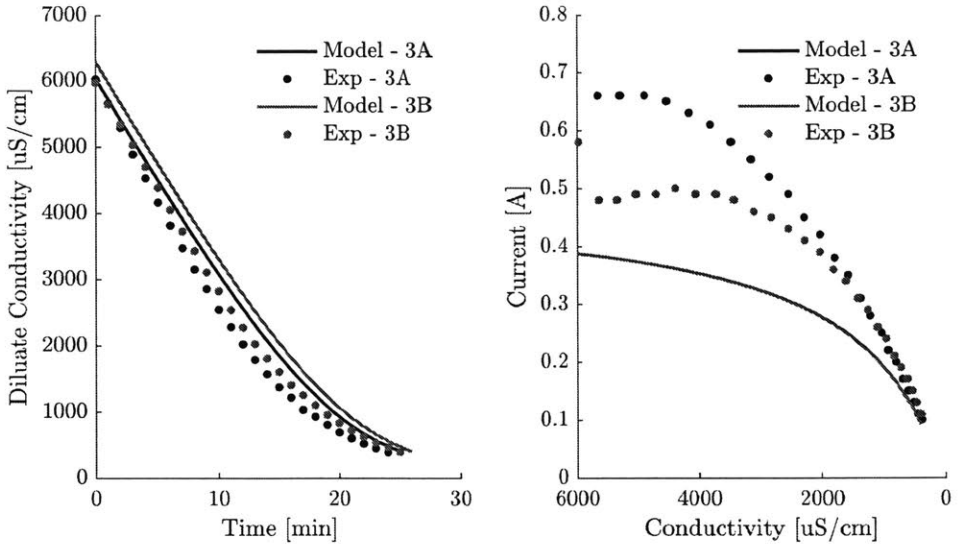

Figure 3-6: Model and experimental diluate conductivity vs time (*left*) and current vs diluate conductivity (*right*) for Test 3. A 3000 mg/L solution was desalinated to 200 mg/L at 80% recovery.

batch process, where the membrane resistance is not dominated by the resistance of the diluate channels. Considering no additional characterization of the membrane was performed prior to testing, the average difference between the predicted and measured production rate of 20% is deemed acceptable for design purposes.

3.3 Pressure Drop

A semi-empirical model was used to predict pressure drop in the channel (Section 2.2.6), because the correlations from Pawlowski *et al.* [37] and Ponzio *et al.* [38] were found to under-predict the pressure drop (Fig.3-7). In order to improve the prediction, the model-form was preserved but a fitting coefficient was introduced in Equation 2.33.

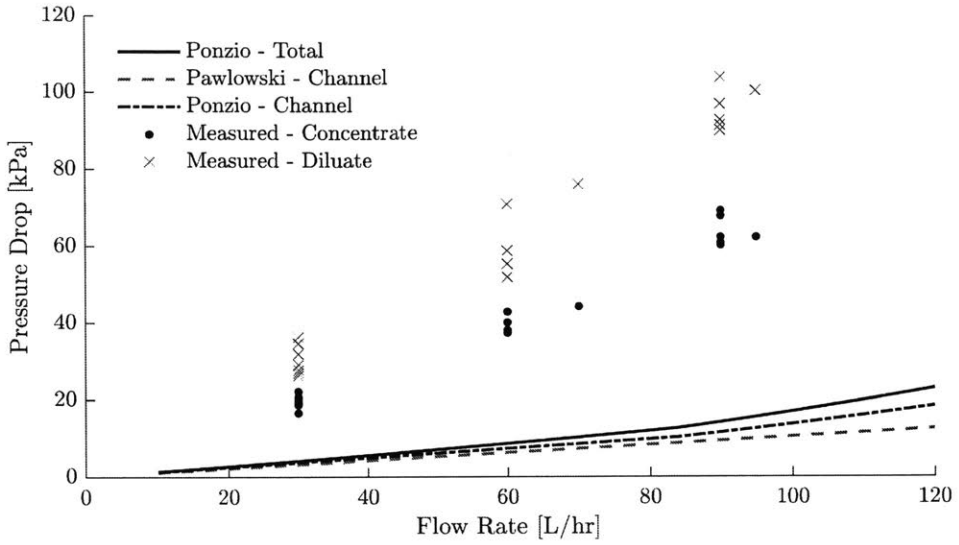

Figure 3-7: The measured pressure drop for the lab-scale test stack (Table 3.1), with 10 cell pairs, was higher than the models proposed in literature[37, 38].

3.4 Summary of Validation Experiments

In this chapter, the accuracy of the models described in Chapter 2 is examined. From the experiments conducted, it is evident that the measured results match closely with the modeled limiting current density and desalination predictions. This strong agreement lends confidence in the simulated performance of candidate ED stack designs, thereby allowing design-iteration and optimization to be performed numerically. While it is not ideal that a fitting parameter was required to improve the pressure drop estimate, the approach provides sufficient accuracy for the purposes of selecting pumps for a system. Future modeling efforts should be directed towards improving the pressure drop prediction analytically, so that the model is applicable to a wider range of ED system scales.

Chapter 4

Cost-Optimization

It was previously discussed in Chapter 1 that Nayar *et al.* have demonstrated that the proposed batch ED system (Fig.4-1) is a viable technology for satisfying household desalination needs, but further cost reduction is required to be competitive with existing RO, devices which are priced between $200-$300. Therefore, in this chapter I investigate the pareto-optimal design of the proposed domestic batch ED system considering production rate, product water concentration, and cost using simulation. In particular, I aim to address the following:

1. How should a domestic ED system be designed to minimize cost?

2. How do water quality and production requirements affect the design?

3. What are the primary contributors to cost?

4. What developments are necessary for further cost reduction?

For this study, we opted to hold the voltage and recirculation flowrates constant during this batch process for two reasons. The first being that it is consistent with the work of others, both in simulation and practice [30, 31, 52, 53], and would therefore provide a good basis for comparing results. However, the second and more significant reason, is that it would facilitate the simplest implementation of ED in a commercial product.

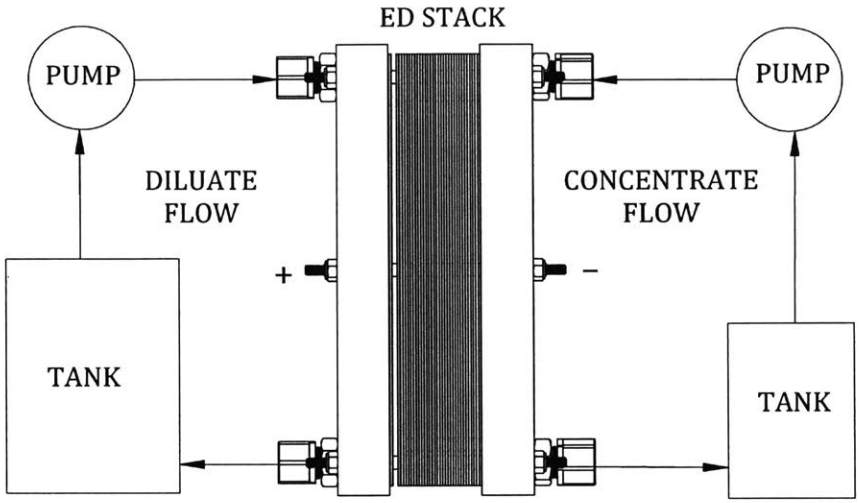

Figure 4-1: Schematic of proposed domestic ED system operating in batch mode.

An additional flow circuit may be required for the electrode rinse stream; however, its design was not considered here because it is not expected to strongly affect desalination performance. Furthermore, for the hybrid ED-RO system investigated by Thampy *et al.*, the RO reject was used to rinse the ED electrodes [26]. It may therefore be possible to integrate the rinse with the concentrate circuit to eliminate a third pump.

Prior design and optimization work has been performed for large-scale systems which are typically operated in a continuous architecture for industrial applications. For these systems, the pump cost and energy consumption could be neglected because they are low relative to cost of the ED stack and the energy consumed by desalination [54, 55]. Optimization at the domestic scale presents a different scenario where the pumps were found to strongly affect the cost, energy consumption, and performance of the ED system.

In addition, minimization of operating costs is often an important consideration in industrial applications whereby the energy consumption can not be neglected [56]. In the present study, it was found that capital cost was the dominant factor affecting the affordability of the domestic system.

4.1 Problem Formulation

Using standard notation, the multi-objective optimization problem being investigated is denoted as

$$\begin{aligned} \min_{\mathbf{x}} \quad & \mathbf{J}(\mathbf{x},\mathbf{p}) \\ \text{s.t.} \quad & \mathbf{g}(\mathbf{x},\mathbf{p}) \leq 0 \\ & \mathbf{h}(\mathbf{x},\mathbf{p}) = 0 \\ & \mathbf{x_{lb}} \leq \mathbf{x} \leq \mathbf{x_{ub}}, \end{aligned} \tag{4.1}$$

where $\mathbf{x}$ is the design vector to be optimized, $\mathbf{p}$ is the vector of constant model parameters, $\mathbf{J}(\mathbf{x})$ is the vector of objective functions, and $\mathbf{g}(\mathbf{x})$ and $\mathbf{h}(\mathbf{x})$ are the inequality and equality constraints, respectively. Each term is detailed in the following sections. In this study, the design vector is bounded from below and above by $\mathbf{x_{lb}}$ and $\mathbf{x_{ub}}$, respectively.

4.1.1 Variables and Bounds

Each design permutation is defined by a design vector $\mathbf{x}$ consisting of the six individual variables listed in Table 4.1 and illustrated in Fig.4-2. The bounds for dimensional variables (L, W, and N) ensure that the proposed system could be packaged within the same envelope as existing domestic RO systems.

Channel heights (h) could vary within the size range of commonly available flow spacers. While thinner mesh thicknesses are available, they are expected to produce pressures (>2 bar) that exceed the capacity of commercially available small-scale pumps in the desired range of flow-rates.

Following the industry-standard operating procedure, equal flow-rates (Q) were prescribed for the diluate and concentrate circuits so that the effects of transmembrane pressure differences could be neglected in this analysis. Then, for equal diluate and concentrate channel dimensions, identical pumps could be used for both streams.

Pumps were not treated as variables. Instead, a pressure drop was calculated for each design iteration. Then, the pump (among the selection provided in Appendix

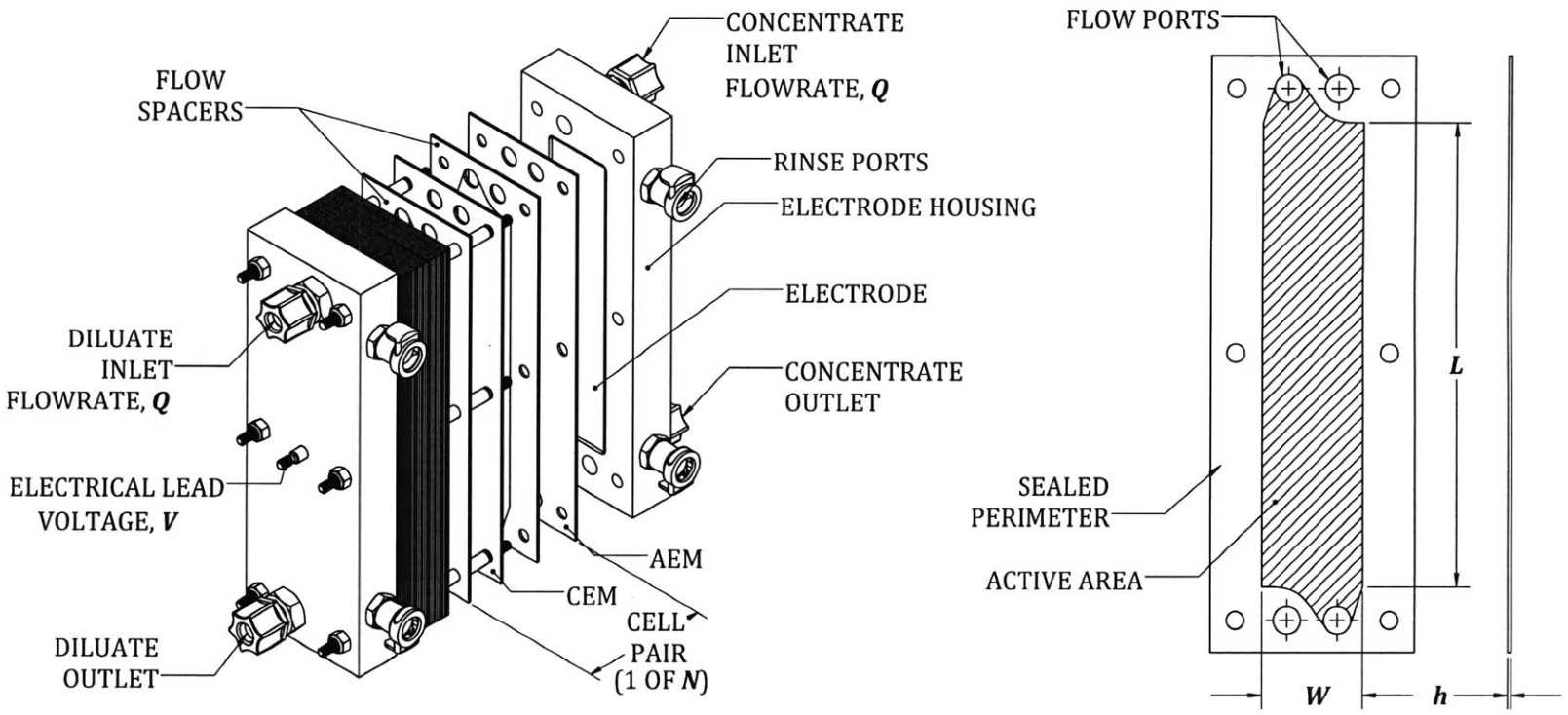

Figure 4-2: Schematic of complete ED Stack (left) and individual flow-spacer (right) indicating variables considered for optimization in bold font.

B) that most closely provided the desired flow-rate served as a reference for power and cost estimation.

Table 4.1: Design Variables and Respective Bounds

Variable	Symbol	Bounds
Length of Active Area	L	2 - 30 cm
Width of Active Area	W	2 - 20 cm
Number of Cell Pairs	N	10 - 30
Channel Height	h	0.30 - 1.00 mm
Flow Rate	Q	10 - 300 L/hr
Voltage	V	5 - 100 V

All variables, including the number of cell-pairs, were treated as continuous due to the limitations of the algorithm implementation (see Section 4.1.5). In practice, the number of cell-pairs would be rounded up to the closest integer from the value recommended by the optimizer.

4.1.2 Objective Function

In this multi-objective optimization problem, the first objective in $\mathbf{J} = [J_1\ J_2]$ was to minimize the total cost of ownership for the proposed domestic ED system. Therefore, J_1 was defined as the total cost TC of the system, given by

$$J_1 = TC = CC + OC \tag{4.2}$$

where CC is the capital cost, and OC is the operating cost. While the quoted unit costs of materials assumed in this analysis likely included a profit-margin for the suppliers, the final vendor's mark-up on manufacturing cost was not considered because it is affected by commercial factors that may vary from one market to another.

Since ED systems are not widely used for domestic desalination, the fouling characteristics and associated maintenance costs are not well-understood. For this reason, the operating cost considered here is only a function of the energy consumption, and given by

$$OC = \mathbb{V}E_s r_E, \tag{4.3}$$

where $\mathbb{V}$ [L] is the total volume desalinated water produced over the assumed product lifetime of 7 years, E_s [J/L] is the specific energy consumption calculated for each design permutation, and the specific cost of electrical energy r_E is approximated at \$0.10/kWh [57].

The capital cost is calculated using the rates provided in Table 4.2. These rates were obtained from wholesale suppliers in order to best estimate the cost at large-scale production. The capital cost for all pumps considered in this optimization study are provided in Appendix B.

Table 4.2: Unit Cost of ED Stack Components

Component	Cost	Reference
Electrodes	\$2000/m^2	[58]
Membranes	\$40/m^2	[59]
Spacers	\$3/m^2	[60]

I intended to capture the minimum active area that satisfied the target production rate and concentration performance. Therefore, the material forming the sealed perimeter (Fig.4-2), which isolates the diluate and concentrate streams and prevents leakage, was not factored into the cost because the thickness of the seal is affected by other design and manufacturing considerations. For example, placing the tie-rods externally to the membranes may allow a thinner seal to be used.

The second objective J_2 is to maximize the rate of desalinated water production Q_p [L/hr], calculated from

$$J_2 = -Q_p = -\frac{V_b r}{t_b}, \tag{4.4}$$

where V_b [L] is the volume in the diluate tank for each batch, r is the recovery ratio, and t_b [hr] is the time to process each batch. The negative sign reflects the desire to maximize production rate.

For most simulations, the product water concentration was treated as a fixed parameter for calculating production rates of design permutations. However, some additional runs were also performed with the product concentration treated as a third objective where

$$J_3 = C_{prod}, \tag{4.5}$$

in order to draw generalizations regarding the effect of product water concentration C_{prod} [mg/L] on cost-optimal design.

4.1.3 Constraints

During the batch simulation, the duration t_{lim} over which the applied current density exceeded 90% (safety factor) of the instantaneous limiting current density was tracked. To ensure that designs operated under the limiting current density, the first inequality constraint in $\mathbf{g} = [g_1\ g_2\ g_3] \leq 0$ to be imposed is

$$g_1 = \frac{t_{lim}}{t_b} - 0.02, \tag{4.6}$$

implying that the safety factor-adjusted limiting current density could not be exceeded for more than 2% of the batch period.

Existing domestic RO products have set expectations for the production rate of desalinated water. As such, we were interested in exploring ED system designs that provided similar production rates (Q_p) in the range of 9-15 L/hr [16, 17]. Therefore,

$$\begin{aligned} g_2 &= 9 \text{ L/hr} - Q_p \text{ and} \\ g_3 &= Q_p - 15 \text{ L/hr}. \end{aligned} \tag{4.7}$$

Lastly, no equality constraints $\mathbf{h}$ were required in this formulation, making the problem easier to solve numerically.

4.1.4 Parameters

Parameters pertaining to the model are provided in Wright *et al.* [61]. Others corresponding to the cost of components and energy have been provided in Table 4.2. In Table 4.3, we provide the remaining parameters relevant to simulation.

The relative sizes of the diluate and concentrate tanks were selected to yield a recovery ratio of 90%, while the actual volumes allowed them to be packaged within

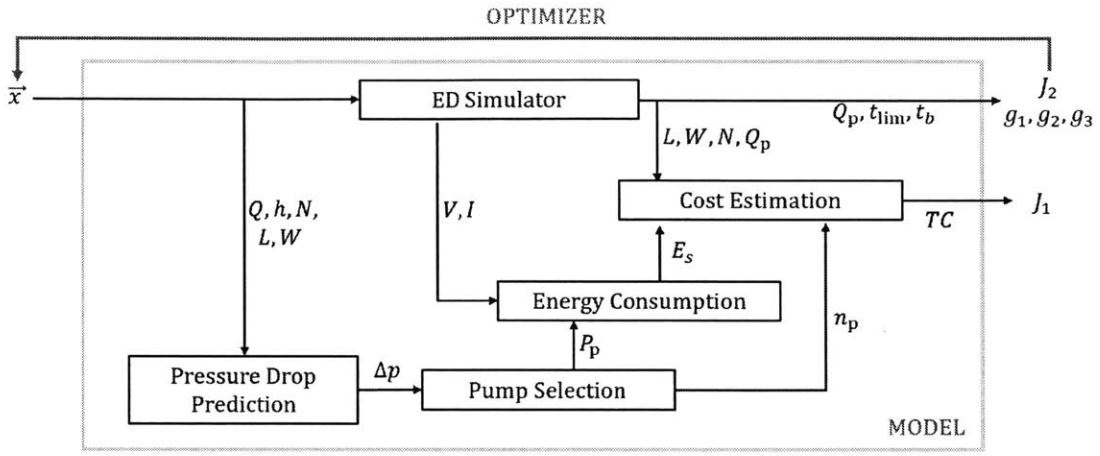

Figure 4-3: Block diagram indicating the flow of design variables between models to calculate the objective function for optimization.

the envelope of existing RO systems. The recovery ratio is maintained at 90% for this study because the purpose of the proposed device is to conserve water.

Table 4.3: Parameters for ED Simulation

Parameter	Value
Feed Concentration, C_{feed}	2000 mg/L
Product Concentration, C_{prod}	100-300 mg/L
Diluate Tank Volume, $\mathbb{V}_{\text{dil}}$	3.6 L
Concentrate Tank Volume, $\mathbb{V}_{\text{conc}}$	0.4 L
Total Volume Produced, $\mathbb{V}$	38 325 L

Solution resistivity was demonstrated to be highly sensitive to concentration changes below approximately 500 mg/L (Fig.2-4); therefore, it was anticipated that the design of an ED system would be more affected by the product water requirements than the feed water concentration. As such, the feed concentration is held fixed at 2000 mg/L, based on the salinity of Indian groundwater [21], for all runs while the product concentration target is varied from 100 to 300 mg/L. The latter range not only satisfies the specifications for water considered suitable for drinking according to the Bureau of Indian Standards [9], but also conforms to the palette of those who are accustomed to drinking RO-filtered water [26].

$\mathbb{V}$ is calculated over the assumed product ownership lifetime of 7 years, based on existing domestic RO device usage, at an average daily drinking water consumption

rate of 3 L/day per person [62] for a household of five members.

4.1.5 Simulation and Optimizer

The block diagram in Figure 4-3 approximates the optimization process, which was implemented in MATLAB [34]. Models pertaining to each block are thoroughly described in 2.

Conventional gradient-based algorithms could not be applied with this formulation because the discrete selection of pumps caused the solution to converge at local minima. Instead, the problem described above was solved using a multi-objective genetic algorithm, specifically the modified NSGA-II algorithm [63] implementation in MATLAB. The solution is a set of non-dominated Pareto optimal solutions with respect to the problem objective functions. The difference between the original NSGA-II [64, 65] and the modified version is that the modified version adds an extra tuning parameter, Pareto Fraction (PF$\in (0,1)$), to control the number of elite members in each population that progress to the next generation. By testing different PFs, we determined that values between 0.5 to 0.75 provided non-dominated solutions without sacrificing convergence speed.

4.2 Results and Discussion

An analysis of the optimal designs obtained for varying production rate and concentration requirements is presented below.

4.2.1 Capital Cost vs Total Cost

Optimal designs that minimized total cost were similar in cost and design to those that minimized capital cost. For example, Figure 4-4 compares the total cost for designs which produce 200 mg/L product water at varying production rates, optimized either for minimum total cost or for minimum capital cost. The former objective function did indeed provide a lower total cost compared to the latter, but the difference of

~$5 was negligible.

This result is explained by comparing the contributions from the operating and the capital cost (Fig.4-4). The operating cost is significantly lower than the capital cost because the cost of electrical energy is small compared to equipment costs, and the system is utilized infrequently. In domestic applications, the system will only be used for 1-2 hours per day depending on the drinking water requirements of the household.

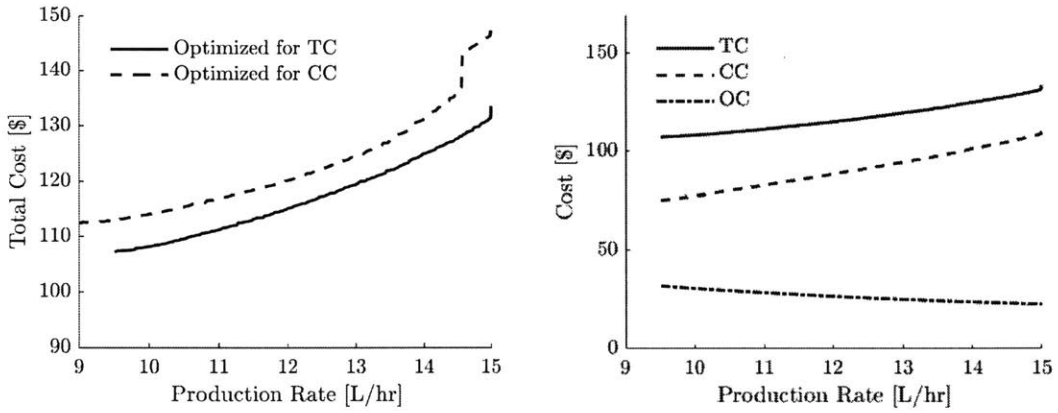

Figure 4-4: Designs optimized for minimum capital cost (CC) had similar total costs to those optimized for minimum total cost (TC) for varying production rates at 200 mg/L product concentration (*left*), because the operating cost (OC) is lower than the capital cost (CC) (*right*).

The design of an affordable domestic ED system is therefore concerned with capital cost minimization. The reader is reminded that this result was obtained even without the inclusion of a mark-up on the capital cost of the system.

The increasing capital cost, and decreasing operating cost, with production rate (Fig.4-4) are explained by examining the current density during the operation of the cost-optimized designs.

4.2.2 Current Density

Maximization of Current Density

It was established in Section 2 that in brackish water ED, the dominant resistance is associated with diluate channels. Since this term is ohmic in nature, the power consumption at a fixed ion removal rate is expected to increase approximately with i^2, where i is the current density. Subsequently, to the first order

$$OC \ \alpha \ i^2. \tag{4.8}$$

However, the required cross-sectional area at the same ion removal rate decreases as

$$CC \ \alpha \ 1/i. \tag{4.9}$$

Since it has been established that the capital cost, which scales primarily with active area (Table 4.2), is the dominant term in the total cost, optimal domestic ED designs are therefore expected to maximize current density. To verify this hypothesis, we examined the ratio of the applied current density to the limiting current density (adjusted by the safety factor n_s=0.9) when the desired product water concentration was achieved (Fig.4-5). This ratio approaches 1 for all optimal designs over a the range of product water concentrations (100-300 mg/L), thereby confirming the aforementioned expectation.

These results agree with McGovern *et al.*'s findings that maximization of the current density was cost-optimal for brackish water desalination using ED at high equipment-to-energy cost ratios [66].

Limiting Current Density Implications

Maximizing the current density is cost-optimal, but there is an upper bound based on the instantaneous diluate concentration and the flow properties (Section 2.1.3). Figure 4-5 demonstrates that the applied current density approaches this limit at the *end* of each batch; however, it is also useful to examine the full duration.

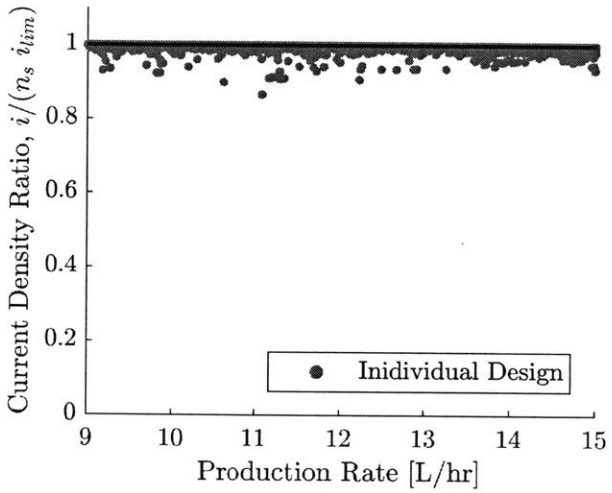

Figure 4-5: Ratio of instantaneous applied current density i to limiting current density i_{lim} at the end of the batch process approaches 1 for all optimum designs targeted at varying product concentrations (100-300 mg/L) and production rates (9-15 L/hr).

For example, the optimal current trajectories during desalination for producing 100 mg/L and 200 mg/L product water at a rate of 10 L/hr are compared in Fig.4-6. Since the **limiting** current density trajectories (solid lines) are similar and mostly dependent on the instantaneous diluate concentration, it is inferred that differences in flow characteristics play a small role here. These upper bounds are only approached at the end of the batch, but the application of a constant voltage constrains the full **applied** current trajectory. Therefore, as is evident in Fig.4-6, relaxation of the product water requirements allows designs to operate at higher current densities for the full batch process.

To further understand the implications of this behavior on cost (Fig.4-7), we examined the time-averaged applied current densities $\bar{i}$ during the operation of optimal designs. The following insights were obtained:

1. With the exception of a few outliers, optimized designs agree with the approximate scaling relationships for the capital cost CC and operating cost OC presented in Eqns.4.8 and 4.9. The y-intercept for the OC trend-line approximates the energetic cost of pumping.

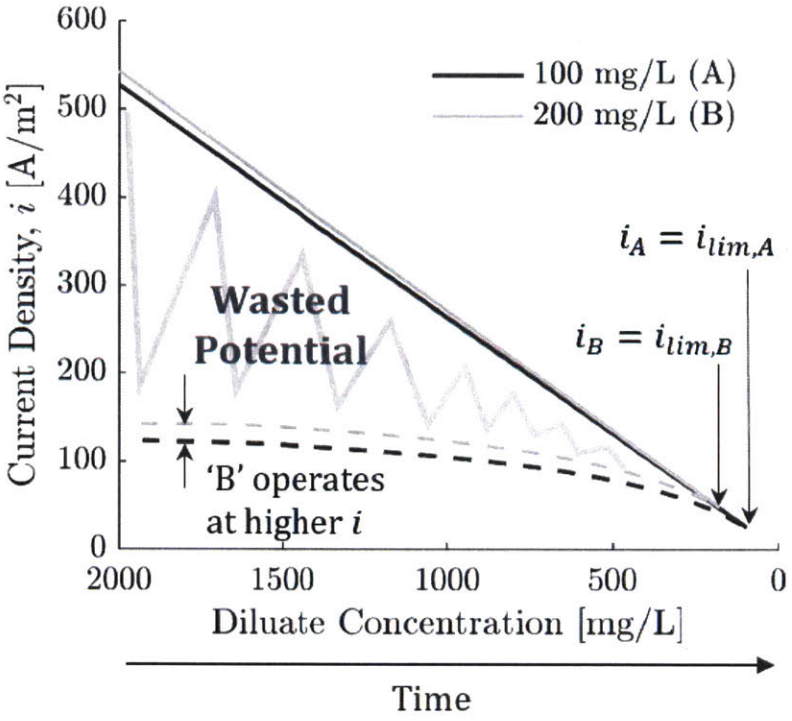

Figure 4-6: Simulated applied current (dashed lines), under constant voltage operation, and limiting (solid) current densities through desalination for designs optimized to produce 200 and 100 mg/L water at 10 L/hr.

2. By extrapolating the CC and OC trend-lines beyond the optimization data, it is speculated that a time-averaged current density $\bar{i}$ of approximately 225 A/m^2 will yield an absolute minimum total cost, which in turn is a function of the specific material and energy costs.

3. Despite the use of optimization, designs targeted at the product concentrations of 100-300 mg/L, at the production rates of interest, lie in the capital cost-dominated region. Hence, the absolute minimum cost can only be achieved by relaxing the product water concentration requirements.

4. Due to the upper bound on $\bar{i}$ imposed by i_{lim}, designs targeted at lower concentrations C_{prod} are further from the absolute minimum cost. Therefore, relaxing the product water requirements allows operation at higher current densities, hence lowering total cost.

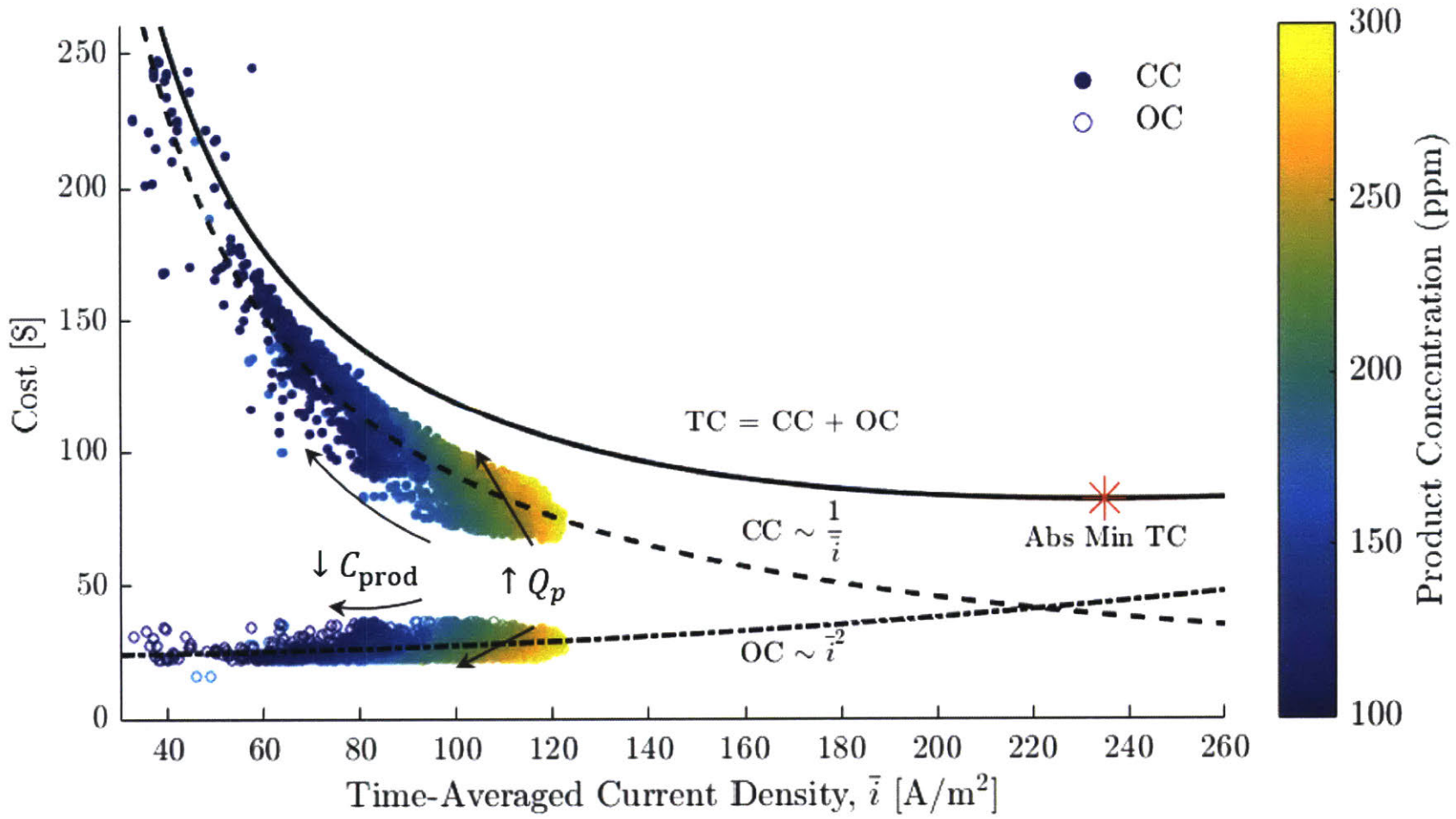

Figure 4-7: Capital cost CC and operating cost OC for optimal designs is plotted against the time-averaged current density $\bar{i}$ during their respective batch operation. Straight and curved arrows indicate direction of increasing production rate Q_p (9 to 15 L/hr) and decreasing product water concentration C_{prod} (300 to 100 mg/L), respectively. Desalination was simulated for 2000 mg/L feed at 90% recovery.

5. Scatter in the data about the trend-lines represents varying production rate requirements. The gradient indicates that increasing the production rate requirements for Q_p from 9 to 15 L/hr also forces operation at lower $\bar{i}$, albeit to a lesser extent than decreasing the product water concentration requirement from 300 to 100 mg/L. As a result, achieving higher production rates also requires an increase in cell-pair area, thereby increasing capital cost. This increase in capital cost exceeds the decrease in operating cost obtained by operating at a lower current density; therefore total cost increases with production rate.

6. The ability to produce low product water concentrations that are comparable to RO (100 mg/L) comes at a significant economic cost. It may be worthwhile to investigate if users would accept product water at higher salinities of 200 to 300 mg/L, which is still suitable for drinking but decreases the system cost significantly.

7. In order to further improve affordability of the proposed batch domestic ED system, the two options are to decrease the unit cost of the components (shifting the CC line down), or to find methods for operating at higher time-averaged current densities (shifting points to the right).

By analyzing Figures 4-6 and 4-7, we discovered that $\bar{i}$ can be increased with time-varying voltage regulation based on measured conductivity of the diluate stream. A high voltage can be applied at the start of the batch process and be gradually decreased to maintain an instantaneous current density that is just under the limiting current density (see Fig.4-6). Since this strategy has the potential to provide significant cost reductions, it is an avenue of ongoing work for our team.

4.2.3 Optimal Design Characterization

In order to minimize capital and total cost of a domestic ED system, it has been shown that the optimal strategy is to maximize the applied current density. We explored how this strategy affected the choice of variable values in order to provide design guidance.

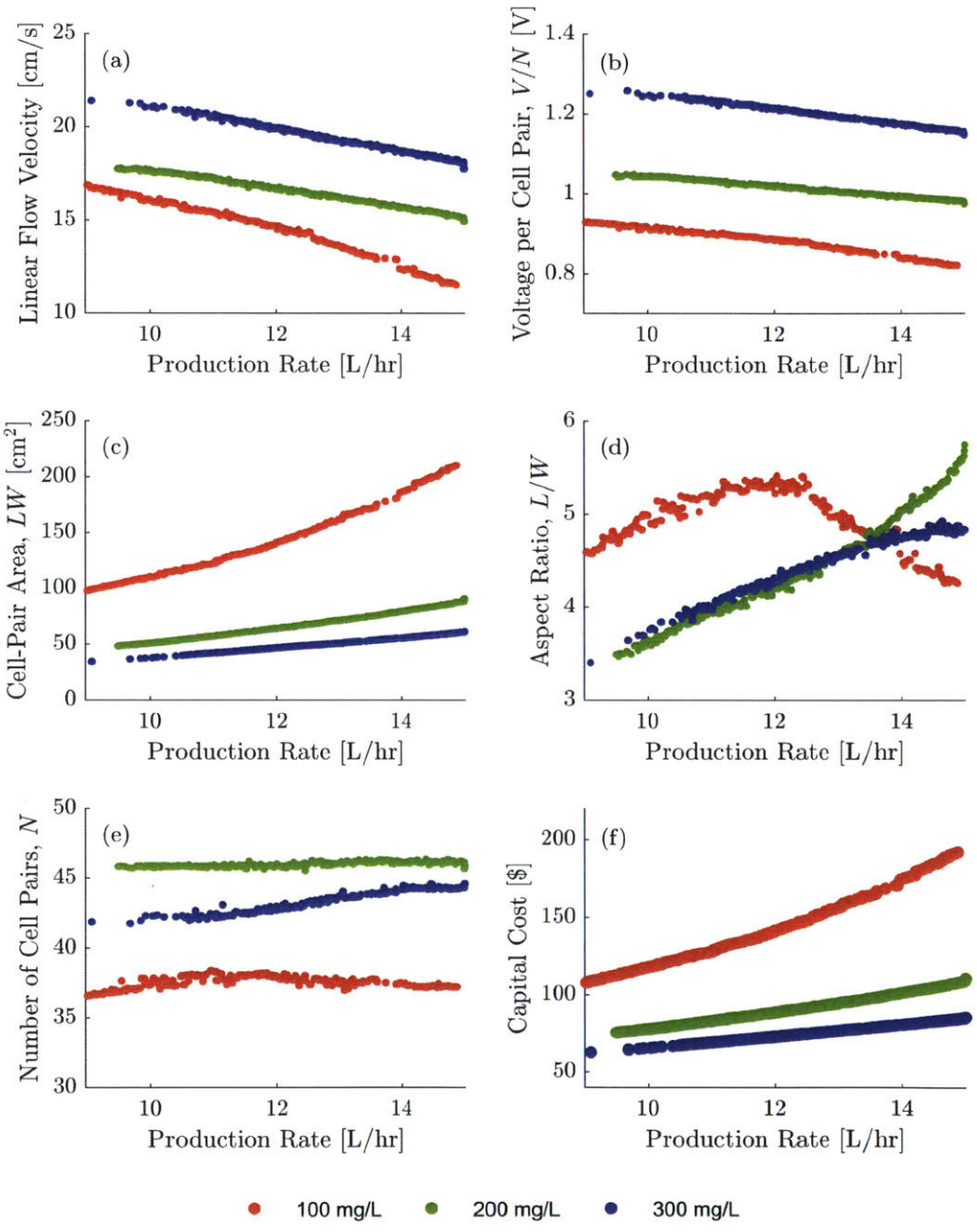

Figure 4-8: Optimal selection of the design variables as a function of the production rate and concentration requirements (a - e). Pareto-optimal capital cost versus production rate for varying product water concentrations (f).

Linear Flow Velocity, u_{ch}

The linear velocity is reported instead of the volumetric flow rate because it is more directly applicable to design, and comparable between different scales of production. Optimal designs operated at 18-21 cm/s for 300 mg/L, 15-18 cm/s for 200 mg/L, and 11-16 cm/s for 100 mg/L product water (Fig.4-8a). These results exceed values used by others in both experimental and theoretical studies, including Lee *et al.* (7.5 cm/s) [55], Tanaka (10 cm/s) [31], and Kim *et al.* (4.24 cm/s) [67]. We postulate that higher linear velocities were not implemented in these cases because the resulting pressures may be difficult to manage for larger systems. As a result, little work has been performed to understand the effect of high flow velocities on desalination performance, fouling behavior, and membrane durability. This work suggests that the development of domestic ED systems may benefit from characterization of these effects.

The decrease in the linear flow velocity with the production rate is explained by the increase in the cell-pair area. The volume flow-rate per cell pair remained approximately constant at 5.1 $\pm$ 0.1 L/hr for the 200/300 mg/L and 6.0 $\pm$ 0.2 L/hr for 100 mg/L, utilizing the maximum capacity of the small-scale pumps used in this investigation. Then, as the width of the active area grew to satisfy higher production rates, the linear velocity decreased.

Voltage, V

In order to avoid exceeding the the limiting current density at the end of the batch, the applied voltage was smaller for designs that targeted lower product water concentrations (Fig.4-8b). Furthermore, the decrease in the applied voltage observed at higher production rates is explained by the decreasing linear flow velocities. Optimal voltage values, ranging between 0.7-1.3 V per cell-pair, agreed with other studies and manufacturer recommendations for concentration ranges similar to those investigated here [27, 30, 31, 68].

Cell-Pair Area, LW

Larger cell-pair area is required to provide the required salt removal rate while compensating for the decrease in the applied voltage (and associated current) at lower concentrations and higher production rates (Fig.4-8c). Both length and width increased with production rate, but the former increased at a faster rate. Inspection of the aspect ratio, defined as L/W (Fig.4-8d), indicates that leaner designs are better-performing because they supply a higher linear flow velocity for a given cell-pair area, thereby facilitating operation at higher current densities, provided that the pumps can sustain the resulting pressure drop. For the 100 mg/L case, a decrease in the aspect ratio was observed after 12 L/hr because the length was prevented from exceeding the upper bound of 30 cm.

Recall that the membrane and spacer material contribution to the seal is not factored into the cost. In practice, implementation of a thick seal will decrease the optimum L/W aspect ratio.

Capital Cost, CC

Capital cost of optimal systems increased nonlinearly with decreasing product water concentration. The difference between 200 mg/L and 100 mg/L systems was greater than from 300 mg/L to 200 mg/L (Fig.4-8f). The sharp increase in the diluate resistance paired with the decrease in the limiting current density with decreasing concentration explains this result. Thus, ED stack architectures targeted at low product concentrations are forced to operate at low current densities applied over larger surface areas to maintain the desired rate of salt removal. These results agree with other work that has found ED to be expensive process for producing ultra-pure water. [66, 69].

Number of Cell-Pairs, N

Implementing more cell-pairs to achieve a higher production rate is not necessarily cost-optimal at the domestic scale (Fig.4-8e). Instead, it was found that the optimal

number of cell-pairs was determined by the capacity of the selected pumps and the required linear flow velocity in the channels.

Channel Heights, h

Smaller intermembrane channel heights decrease the electrical resistance of the channels (Eqn.2.10) and increase the mass transfer coefficient (Eqns.2.15-2.17). Optimum heights approached the lower bound of the variable, ranging between 0.30 - 0.33 mm for the full spectrum of production rates and concentrations analyzed in this study. This result signifies that the enhanced mass transport provided by thin channels justified the cost of greater pressure drop over the design space and range of operation considered in this study.

4.2.4 Cost & Energy Breakdown

Figure 4-9 distributes the capital cost of optimal systems providing between 11.5 and 12.5 L/hr of production into average contributions from components. Pumps accounted for a significant fraction, particularly at 200 and 300 mg/L. The remainder was balanced between electrodes and membranes.

Comparison across the concentrations indicates that there is a significant economic penalty for producing water at the lowest salinity of 100 mg/L. Again, this observation suggests that it may be prudent to reassess users' reception toward 300 mg/L water and whether their preference for 100 mg/L justifies the significant cost addition.

A similar breakdown is provided for energy consumption due to desalination and pumping (Fig.4-9). Here, pumps accounted for as high as 83% of the total energy consumption. In addition, the contribution from desalination did not vary significantly with product concentration, hence mirroring the slow growth of OC with $\bar{i}$ in Figure 4-7.

Overall, this work has indicated that the development of low-cost and energy efficient pumps that are suitable for flow-rates ranging between 200 and 300 L/hr, while sustaining pressures up to 2 bar, will assist the commercialization of domestic

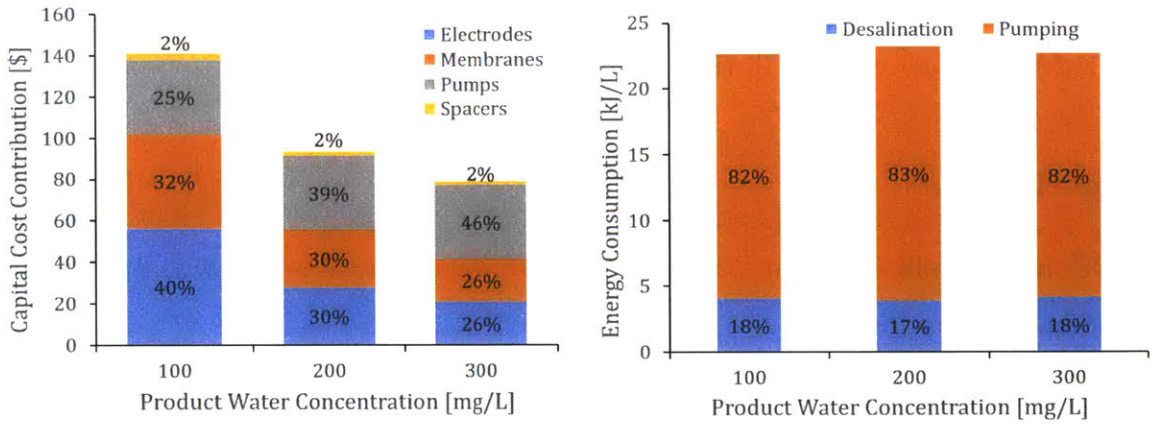

Figure 4-9: Average capital cost (*left*) breakdown and energy consumption (*right*) for all optimal systems producing 11.5-12.5 L/hr at different product concentrations.

ED systems. In addition, a more detailed investigation surrounding the optimal geometry of flow-spacers may provide similar or better mass transfer behaviour at a lower pressure drop, thereby also reducing the pumping expense.

4.3 Summary of Findings from Cost-Optimization

Cost-optimal designs of batch ED systems that met the desalination requirements of a household was investigated through the use of a multi-objective genetic algorithm in this chapter. Production rates (9-15 L/hr) and product concentrations (100 - 300 mg/L) that matched the expectations of existing domestic RO users were targeted at a fixed feed concentration of 2000 mg/L and 90% recovery. Voltage and flow-rates were held constant during the batch desalination process for each design.

In all cases, capital cost was found to dominate over the operating cost due to the upper-bound on the ion removal rate imposed by the limiting current density. Hence, optimal designs under constant-voltage operation were unable to provide the minimum total cost given existing equipment and energy costs. Furthermore, deviation from this absolute minimum increased when the target product water concentration was lowered. Therefore, while batch ED can be used to produce 100 mg/L water, the capital cost of optimal designs remained significantly higher than alternatives targeted at 200 and 300 mg/L.

To maximize the current density during operation, thin channels (0.30-0.33 mm), high aspect ratios (3.5 - 6), and cell-pair numbers that varied from 36 to 46 were recommended. Voltages applied to larger systems were found to be applicable at the domestic scale; however, optimal flow velocities (11 - 21 cm/s) were greater than reported in other literature. Other details, including the cell-pair area, have also been provided to guide the design of domestic ED systems.

By analyzing the limits of the optimized designs we have also identified three directions that can further increase affordability to facilitate commercialization: voltage regulation during the batch process, development of inexpensive pumps suited to this application, and a detailed investigation on optimal spacer geometry.

The primary limitation of this work is the exclusion of membrane replacement expenses in the operating cost. Since the cost-optimal approach was to minimize cell-pair area, the corresponding membrane replacement cost would also be therefore minimized. However, operating at the suggested high linear flow velocities may negatively impact membrane life, and subsequently increase replacement frequency. Therefore, further experimental work to characterize membrane performance is also recommended.

THIS PAGE INTENTIONALLY LEFT BLANK

Chapter 5

Prototype Fabrication and Testing

Initial design of the proposed batch ED system for home-scale was performed primarily using simulation and numerical optimization. An optimal design solution was selected for prototyping thereafter, and evaluated against the targeted production rate and concentration specifications. The prototype specifications, fabrication methods, and test results are presented in this chapter. By verifying the measured performance against predictions, the models and optimization scheme presented in Chapters 2 and 4, respectively, are also validated for use in further design exploration. Lastly, fabrication of the physical system elucidated other practical considerations which are not captured in simulation models.

5.1 Prototype Specifications

From the optimization results, a system that desalinated from 2000 mg/L to 200 mg/L at 10.1 L/hr of production was selected for prototyping. However, due to manufacturing difficulties, the number of cell-pairs in the actual implementation was decreased to 20 from the requirement of 43. The voltage and flow-rate per cell-pair were maintained as calculated from the optimization study, causing the expected desalination rate to linearly decrease from the above expectation to 4.7 L/hr (Table 5.1).

Table 5.1: Design Parameters for Prototyping and Expected Production Performance

Design Parameter/Performance Target	Specification
Width	3.6 cm
Height	16.6 cm
Channel Thickness	0.35 mm
Number of Cell-Pairs	20
Voltage per Cell-Pair	1.0 V
Flow-rate per Cell-Pair	5.4 L/hr
Feed Water Concentration	2000 mg/L
Product Water Concentration	200 mg/L
Drinking Water Production Rate	4.7 L/hr
Recovery Ratio	90%

5.2 Fabrication

Materials and processes used for constructing the prototype (Fig.5-1) are provided in Table 5.2.

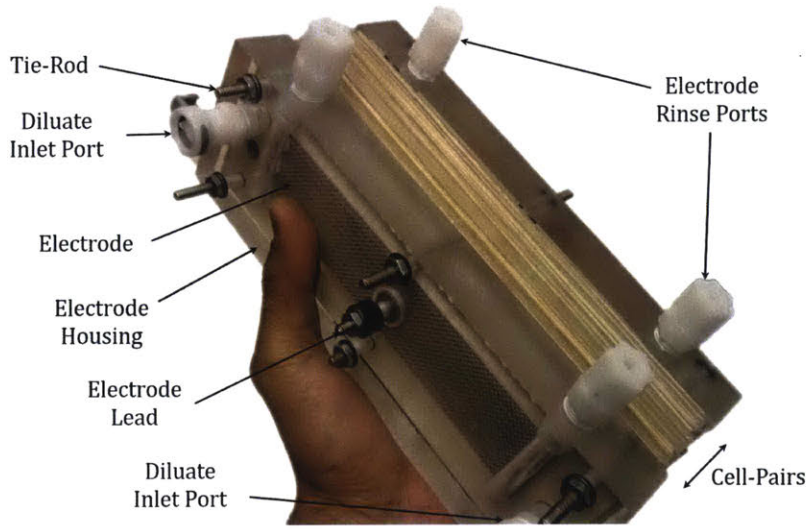

Figure 5-1: Prototype ED stack, with components labeled. Not shown here are the concentrate inlet and outlet ports, along with the other electrode on the far side of the stack.

Fabrication of the spacers posed the greatest challenge. An effective seal was required along the perimeter of the spacers, but the dimensions of the enclosed active area was to be also repeatably controlled within 1-2 mm of the design specifications.

Table 5.2: Prototype Materials and Fabrication Processes

Component	Material	Fabrication Methods
Electrode	316SS Mesh (McMaster, 9319T154) with 316SS Shoulder Screw Electrical Lead (McMaster, 97345A542)	Cut to size from mesh stock, and micro-TIG welded the electrical lead on custom jig (Fig.5-2B).
Electrode Housing	1" Acrylic Block (McMaster, 1227T659)	Machined
Spacers	0.35 mm Polypropylene Woven Mesh (Industrial Netting, WN0500-72P)	Masked with adhesive-backed paper, laser-cut to size (Fig.5-2A), and sealed using a food-safe resin (Smooth-On, Sorta Clear 37).
Membranes	CEM and AEM (Membranes International, AMI-7001 & CMI-7001)	Soaked, cut to size, and post-drilled holes.
Tie-Rods	316SS Threaded Rod (McMaster, 90575A367)	-
Flow Ports	Quick-release Nylon Fittings (McMaster, 5694T141 & 5923K21)	-
Flow Pumps	Diaphragm Pumps (Singflo 2401)	-
Rinse Pump	Diaphragm Pump (Singflo 2203)	-

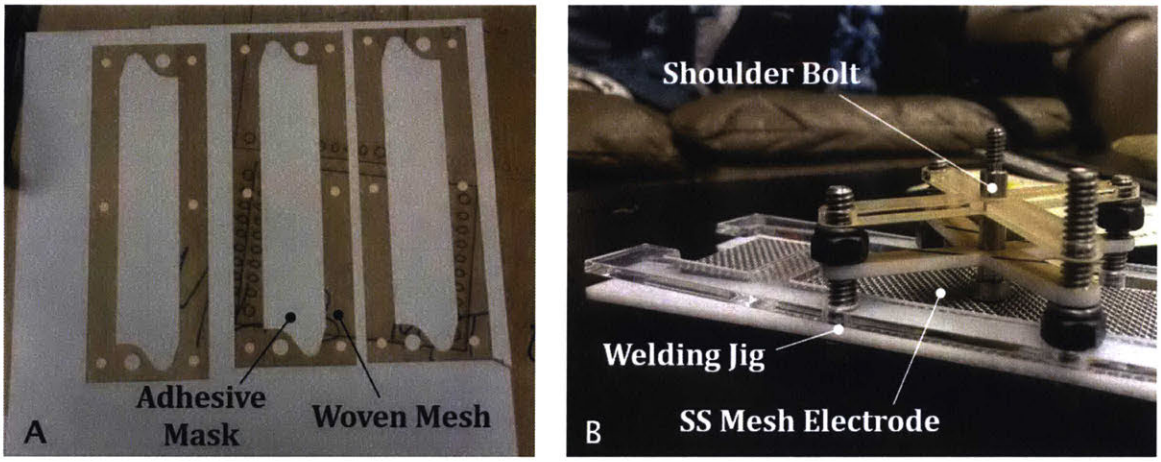

Figure 5-2: The woven mesh was covered with an adhesive, which was subsequently selectively laser-cut to produce a mask prior to applying sealant (A). A shoulder-bolt, which acted as the electrical contact lead, was welded onto the 316SS mesh using a custom-made jig (B).

The approach of laser-cutting a mask (Fig.5-2A), that could be removed after sealant was applied, provided desirable results. However, further experimentation with curing

under a vacuum, or between plates, is recommended to improve control over the the seal thickness.

An additional difficulty was encountered with preparing the membranes. Once soaked, the membranes expanded approximately 15%, causing the dimensions to change. Cutting the dry membrane to the required dimensions resulted in the dislocation of its flow-ports once it was wet. It is therefore critical that dimensions be adjusted for this linear expansion if the membrane is sized in the dry state. An alternative approach, which was implemented with the fabrication of this prototype, is to size and drill the flow-ports once the membrane was already soaked.

5.3 Testing

Testing of the prototype was performed at the GEAR Lab, and at the collaborator's testing facility - Aquadiagnostics - in Bangalore, India. The experimental set-up, test procedure, and results are discussed in the following sections.

5.3.1 Desalination Tests at GEAR Lab

Desalination tests using pure NaCl solutions were performed at the GEAR Lab. A similar experimental set-up (Fig.5-3) to that schematized in Figure 3-1 was used, deviating only in the use of a 2000 mg/L NaCl solution for the electrode rinse rather than a sodium sulfate solution. As indicated in Table 5.3, the only parameter that was varied between tests was the applied voltage. While a recovery ratio of 90% was targeted, the actual recovery ratio was 86% after the additional fluid in the piping was accounted for.

The measured desalination rate matched closely with model predictions (Fig.5-4). Given the diluate volume of 1.8 L, the production rate for a product water concentration of 200 mg/L at the design voltage of 20 V is interpolated to be 4.8 L/hr from the measured results. This value is within 2% of the targeted performance (Table 5.1).

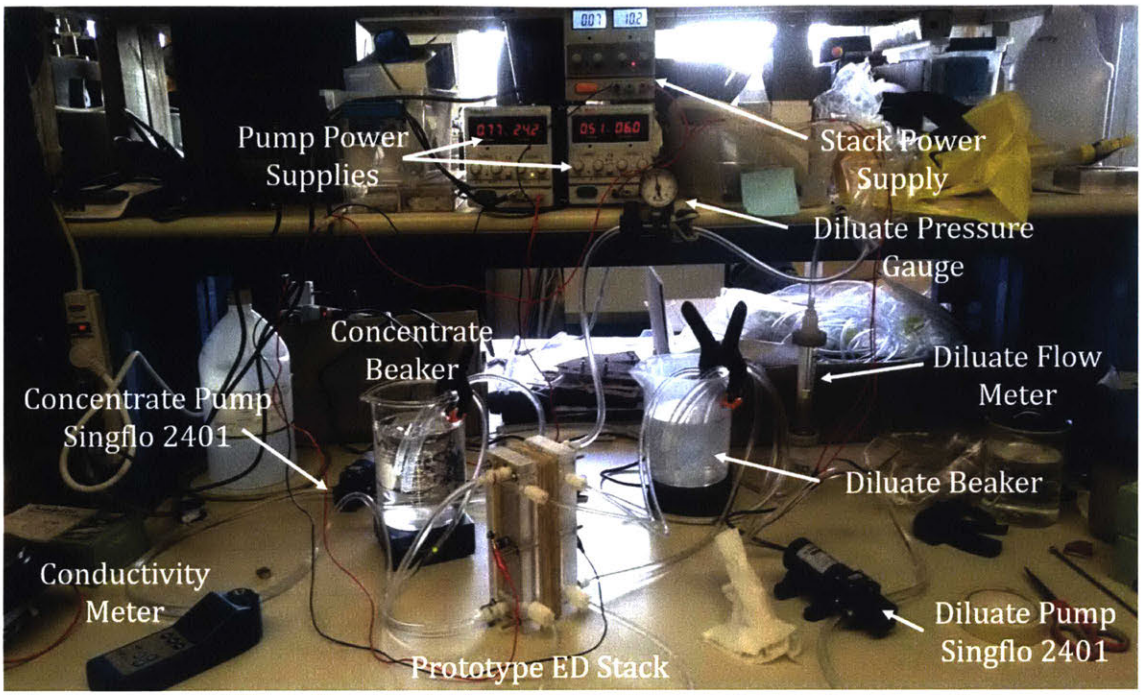

Figure 5-3: Experimental set-up used to test the prototype at the GEAR Lab. Note that the rinse stream network is not shown in this image.

From the strong agreement between the measured and modeled conductivity profiles, one would expect the measured current to also match closely with the predicted current. However, the measured current was consistently higher than expected through all tests (Fig.5-5). Inspection of the membranes revealed signs of tie-rod corrosion (Fig.5-6). Due to imperfect sealing, the tie-rods provided an electrical path that was parallel to the cell-pairs. Therefore, the additional current traveling through the tie-rods resulted in a higher total current being measured.

Table 5.3: Prototype NaCl Desalination Test Parameters

	Test 1	**Test 2**	**Test 3**
Stack Voltage [V]	18	22	26
Flow-rate [L/hr]	100		
Feed Concentration [mg/L]	2000		
Product Concentration [mg/L]	100		
Diluate Volume [L]	1.8		
Concentrate Volume [L]	0.2		
Recovery Ratio [%]	86		

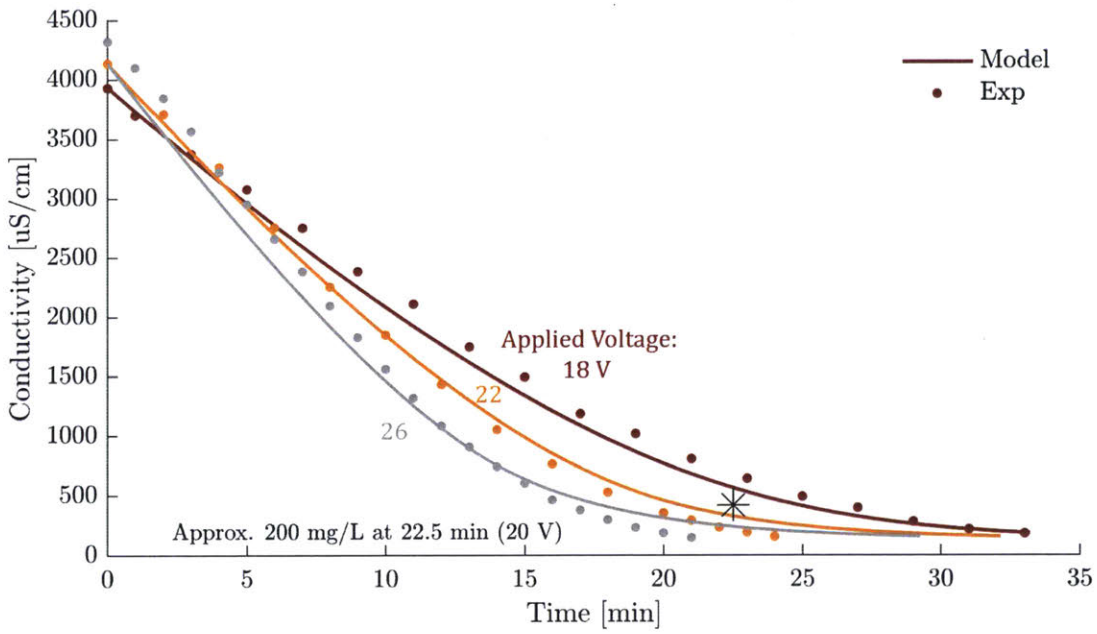

Figure 5-4: Model-predicted diluate conductivity profile is compared against the measured diluate conductivity through time, obtained with the prototype at varying applied voltages. At the design voltage of 20 V, a concentration of 200 mg/L would be achieved in approximately 22.5 minutes.

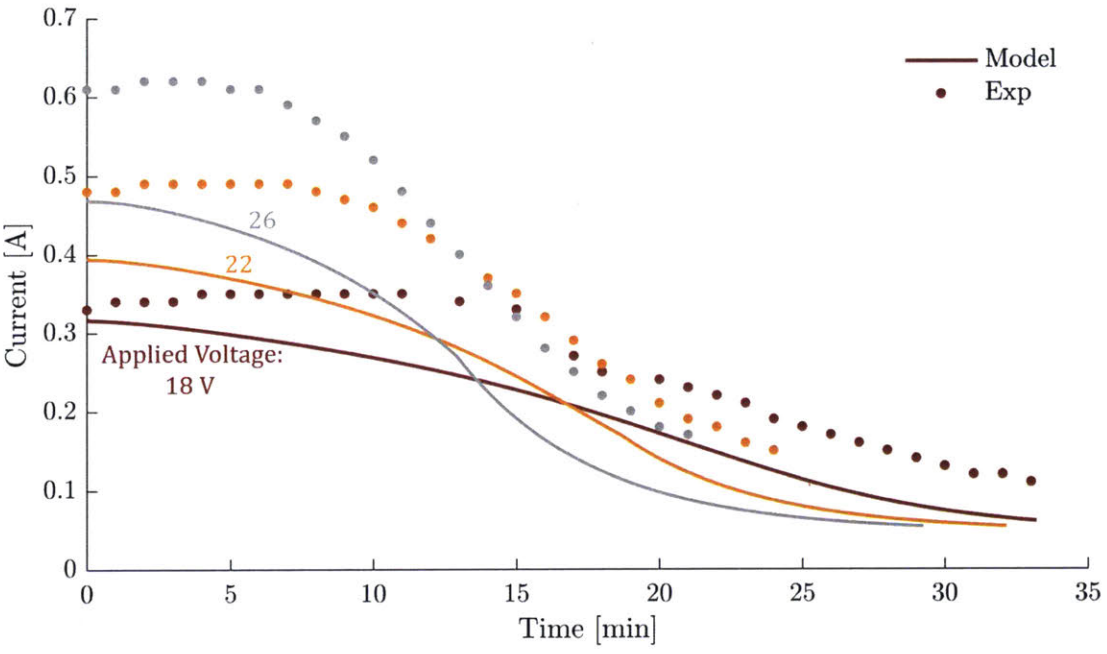

Figure 5-5: The measured current was greater than the predicted current for the prototype in all tests.

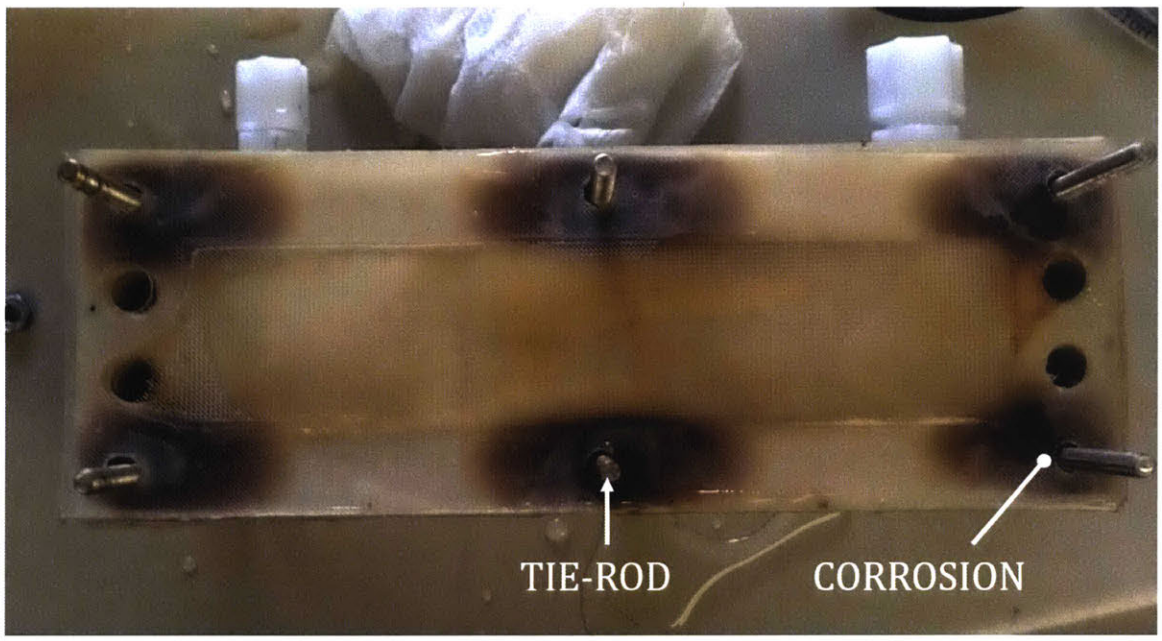

Figure 5-6: The corrosion of the tie-rods indicate that they provided an electrical path, parallel to the cell-pairs, for the the current to travel through.

5.3.2 Desalination Tests at EFL/Aquadiagnostics

The prototype performance was also tested against untreated water obtained directly from a bore-well at the Aquadiagnostics testing facility (Table 5.4). Using a hand-held TDS meter, it was shown that the prototype successfully desalinated 7.7 L of water from 960 mg/L to 200 mg/L within 60 minutes at 89% recovery, hence providing a production rate of 7.7 L/hr (Fig.5-7). Since the water composition is unknown, it is not possible to model the prototype's performance and make a comparison with the experimental results.

Table 5.4: Aquadiagnostics Test Parameters

Parameter	**Value**
Stack Voltage [V]	24
Flow-rate [L/hr]	100
Feed TDS [mg/L]	980
Product TDS [mg/L]	100
Diluate Volume [L]	7.7
Concentrate Volume [L]	1
Recovery Ratio [%]	89

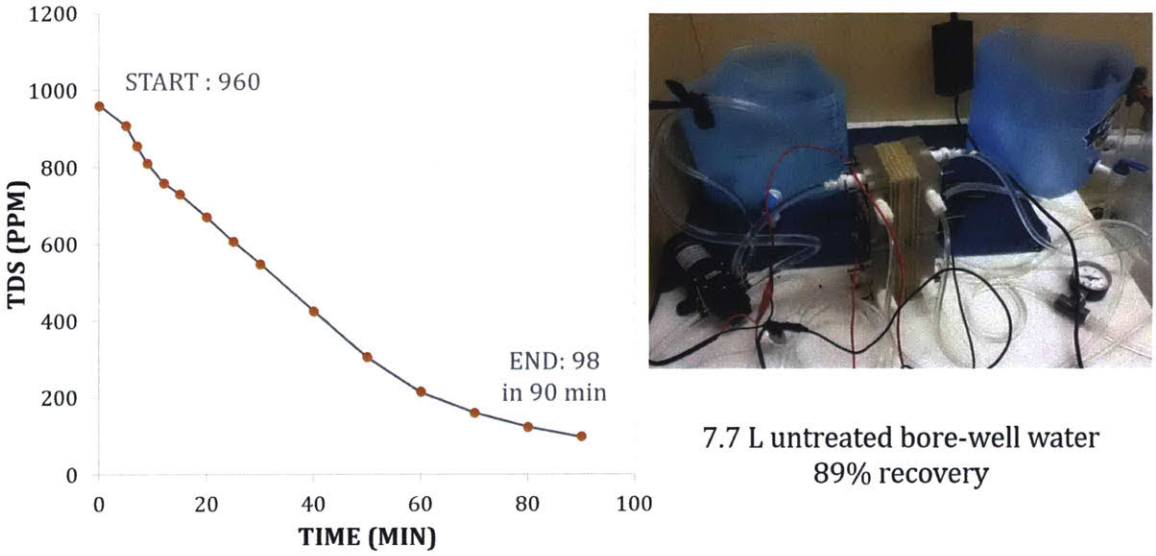

Figure 5-7: A test using untreated bore-well water was performed at the Aquadiagnostics testing facility (*right*). The TDS of the diluate, treated by the prototype, was measured against time (*left*).

5.3.3 Limiting Current Density

The same test procedure outlined in Section 3.1 was implemented, but a change in the slope of the current-voltage plot was not observed under any operating conditions (Fig.5-8). Failure of this test is attributed to the poor sealing of the electrodes, as discussed above in Section 5.3.1. Since the electrodes provided a parallel path for current flow, the measured current was not exclusively related to ion transfer across the exchange membrane. Specifically, it was not possible to observe the point at the depletion of ions at the membrane resulted in the decomposition of water molecules.

5.3.4 Pressure Drop

An independent pressure-drop test was not conducted. However, pressure-drop was recorded while performing desalination and limiting current density tests. The measured pressure drop was found to closely agree with predictions from the model (Fig.5-9). This verification indicates that it is appropriate to use the previously described pressure drop model (Section 2.2) to select pumps that facilitate operation of the batch ED system at the desired flow-rates.

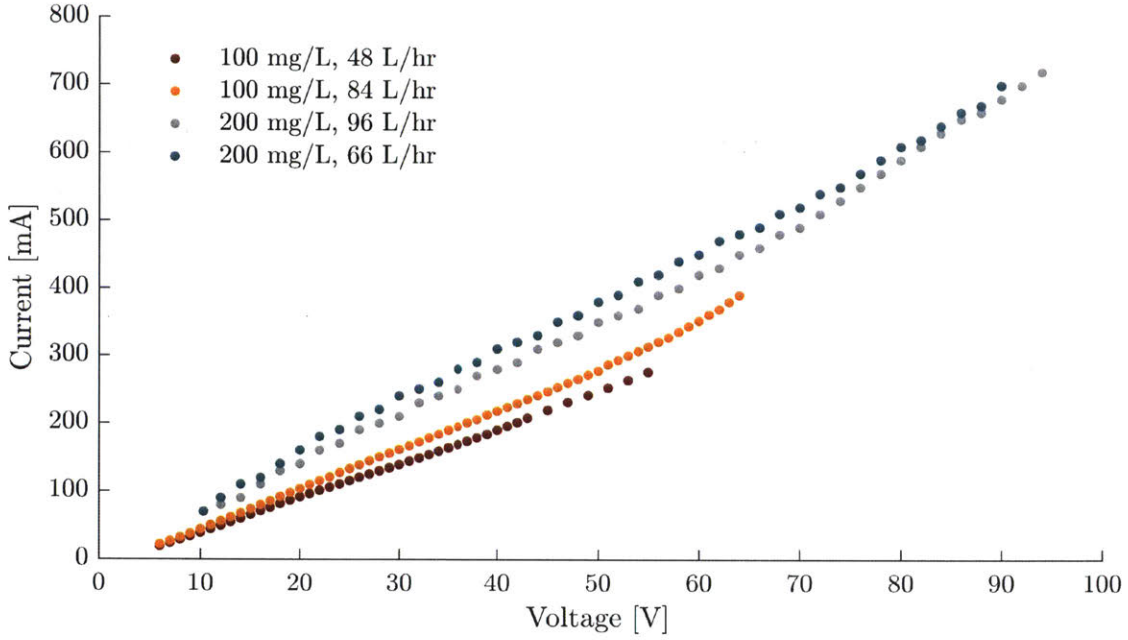

Figure 5-8: Current is plotted against voltage applied across prototype stack with solutions of varying concentration circulated at varying flow-rates. No noticeable change in slope was observed; therefore, the limiting current could not be determined using this approach.

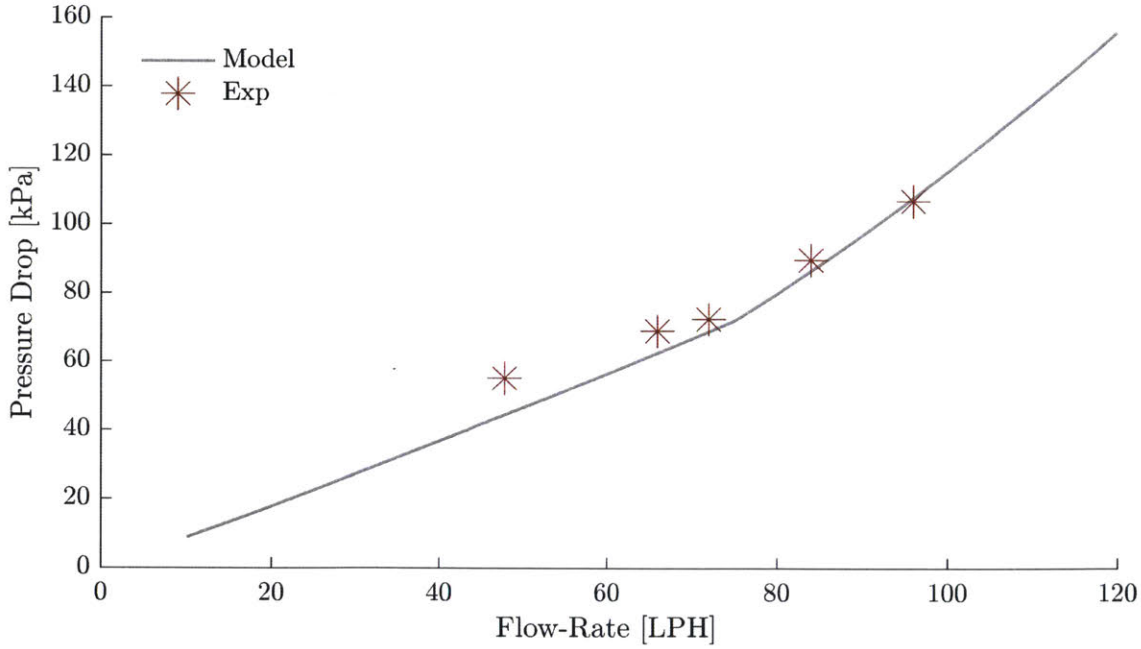

Figure 5-9: Comparison of the measured pressure drop against the model-predicted system curve for the prototype with 20 cell pairs.

5.4 Summary of Prototype Performance and Suggested Improvements

This chapter evaluates the performance of a prototype which was optimized for producing 200 mg/L water from 2000 mg/L at 4.7 L/hr and 90% recovery, using the models and optimization methods presented in Chapters 2 and 4, respectively. While the desalination rate and pressure drop measured for the prototype closely matched expectations, limiting current density tests could not be performed due to inadequate sealing and subsequent corrosion of the tie-rods. In addition to resolving this problem, the following improvements are suggested for future prototype iterations.

- Stainless steel electrodes were used for both the anode and cathode. As anticipated, this necessitated the use of a separate rinse stream to prevent the corrosion from contaminating the diluate and concentrate streams. One should strive to use platinized titanium electrodes in future prototypes to eliminate the need for this third flow circuit.

- The use of plastic tie-rods, or tie-rods that are external to the spacers, will eliminate corrosion.

- By using tie-rods that are external to the spacers, it may also be possible to reduce the size of the seal.

- The membranes could not be laser-cut, since the process would release toxic fumes. As a result, membranes were manually cut for this prototype; however, this resulted in poor dimensional repeatability. A stamping process is recommended for future prototypes.

- It may be possible to integrate the rinse and concentrate streams internally within the ED stack in order to eliminate the four rinse flow-ports.

Chapter 6

Conclusions and Future Work

This thesis investigates how a batch ED system can be designed to satisfy the desalination requirements of households in Indian cities at the lowest total cost. This work has involved the identification of performance specifications derived from existing Reverse Osmosis (RO) products and user interviews, the development of coupled flow-mass transfer models to predict the performance of a proposed design, calculation and exploration of the pareto-optimal design space addressing total cost, product concentration, and production rate, and prototyping of a candidate configuration.

The lack of public provisions for clean drinking water, and reliance on brackish groundwater, has resulted in wide-scale adoption of household RO water purification and desalination systems in urban India. The role of the RO membrane in these devices is primarily desalination, whereby replacement with electrodialysis (ED) can increase recovery from 25-40% to 80-90%, and reduce energy consumption attributed to both desalination and pumping water to above-ground tanks.

A target specification for the proposed ED desalination system was generated by considering the user's preference for low salinity drinking water of approximately 100 mg/L, below the requirement of the Indian Bureau of Standards of 500 mg/L, along with production rate (9-15 L/hr), size, and storage (8-10 L) based on existing RO capabilities. With assistance from Eureka Forbes Ltd, a leading manufacturer of household water purifiers in the Indian market, a capital cost objective of $75 was established as being competitive with RO.

After evaluating previous attempts found in literature at developing such a system, a batch architecture was selected over a continuous one as being more suitable for this application since it provided the ability to desalinate at a high recovery in a compact configuration, thereby resulting in lower cost. A coupled flow-mass transfer model was developed to predict the desalination rate of an ED stack in this architecture, given its geometry, flow, and voltage parameters, and validated on a lab-scale stack. In addition, pressure drop through the stack was predicted in order to estimate the capital cost of pumps that provided the design flow-rate, as high as 46% of the system's capital cost is attributed to the pumps at this size scale.

Cost-optimal designs were calculated with the use of a multi-objective genetic algorithm, for varying production rate (9-15 L/hr) and product water concentrations (100-300 mg/L), while maintaining 2000 mg/L feedwater and 90% recovery. The decrease in limiting current density and conductivity caused the capital cost to increase sharply for 100 mg/L systems: \$141 vs. \$93 and \$79 for 200 mg/L and 300 mg/L systems, respectively averaged for systems that produced between 11.5 and 12.5 L/hr of desalinated water. The optimal voltage varied from 0.9 to 1.3 V per cell-pair from 100 to 300 mg/L systems at 9 L/hr of production, and decreased thereafter. Large cell-pair length-to-width aspect ratios (3.5:1 to 6:1) and thin channels (0.30-0.33 mm) promoted high current densities. Most notably, the optimal linear velocities ranged between 11-21 cm/s, 2-5 times greater than suggestions found in literature for larger systems. Lastly, higher production was obtained primarily by increasing cell-pair area rather than the number of cell-pairs, which ranged between 36-46.

A candidate design targeted at 200 mg/L product water was prototyped to compare the measured desalination output against modeled expectations, and elucidate practical considerations not captured by simulation. Operating with a reduced number of 20 cell-pairs, each measuring 3.6 cm x 10.6 cm, feedwater at 2000 mg/L was desalinated to 200 mg/L at 4.8 L/hr, which was within 2% of the expected production rate at an applied voltage of 1.0 V/cell-pair. Improving the processes for sealing spacers and cutting membranes will allow future prototypes to be tested with the design number of cell-pairs without water leakages and tie-rod corrosion.

In addition to guiding the design of domestic ED systems, this work has also identifies the following other directions for further cost reduction.

- *Voltage regulation during the batch process.*

  Following common industry practice, voltage was held constant during the batch duration. However, voltage regulation based on diluate conductivity will allow operation at higher current density, and consequently reduce the required cell-pair area.

- *Lower-cost pumps.*

  The capital cost contributions from the pumps was 26-40% for optimal systems producing between 11.5-12.5 L/hr. The development of inexpensive pumps will result in significant cost reduction.

- *Spacer geometry*

  This work takes a limited approach to modeling the effect of the spacer on mass transfer and pressure drop properties. A more detailed investigation may identify spacer geometries that facilitate operation at higher current densities at the cost of lower pressure drop.

- *Detailed characterization of taste preferences.*

  A severe cost penalty is incurred by decreasing the product water salinity requirements from 300 mg/L to 100 mg/L. A better understanding of the customers' tolerance for higher salinity, or sensitivity to specific ions may allow this requirement to be relaxed.

THIS PAGE INTENTIONALLY LEFT BLANK

Appendix A

Estimate of Water Transport Rate

In Chapter 2, water transport due to osmosis and electro-osmosis is neglected in the model because under the assumption that it is small compared to the targeted production rate. Here, an estimate of the water transport rate is provided to verify this assumption.

The mass flux of water J_w from the diluate to the concentrate channels due to electro-osmosis (first term) and osmosis (second term) is

$$J_w = M(\frac{T_w i}{F} + D_w \Delta\pi), \tag{A.1}$$

where M is the molar mass of water (18 g/mol), T_w is the water transport number ($\sim$ 9.1 [32]), i is the current density ($\sim$ 50 A/m^2 from Figure 4-7), F is the Faraday constant (96485 C/mol), D_w is the permeablity of the membrane to water ($\sim$ 1.4 x 10^{-4} mol/bar-m^2-s [66]), and $\Delta\pi$ is the difference in the osmotic pressure across the membrane, whereby

$$\Delta\pi = \phi z R T \Delta C. \tag{A.2}$$

R (8.314 x 10^{-5} bar-m^3/mol-K) is the gas constant, and assuming the solution contains only sodium-chloride at room temperature (T = 300 K), the number of ions produced during dissociation z is 2. Lastly, the osmotic coefficient ϕ is approximately 0.9.

For a feed concentration of 2000 mg/L and a recovery of 90%, a diluate concentration of 100 mg/L will yield a concentrate concentration of 19100 mg/L. Then, with the corresponding concentration difference across the exchange membranes of $\Delta C = 325$ mol/m^3, the calculated rate of water transport is 0.124 g/m^2-s. Assuming a 20 cell-pair stack with 8 cm x 8 cm cell-pairs, similar to the one used by Nayar *et al.* [27], the total water transport is approximately 57 mL/hr. Note that this value is on the order of 100 times smaller than the production rate of 10 L/hr, hence it is valid to assume that water transport during desalination is negligible.

Appendix B

Pump Selection

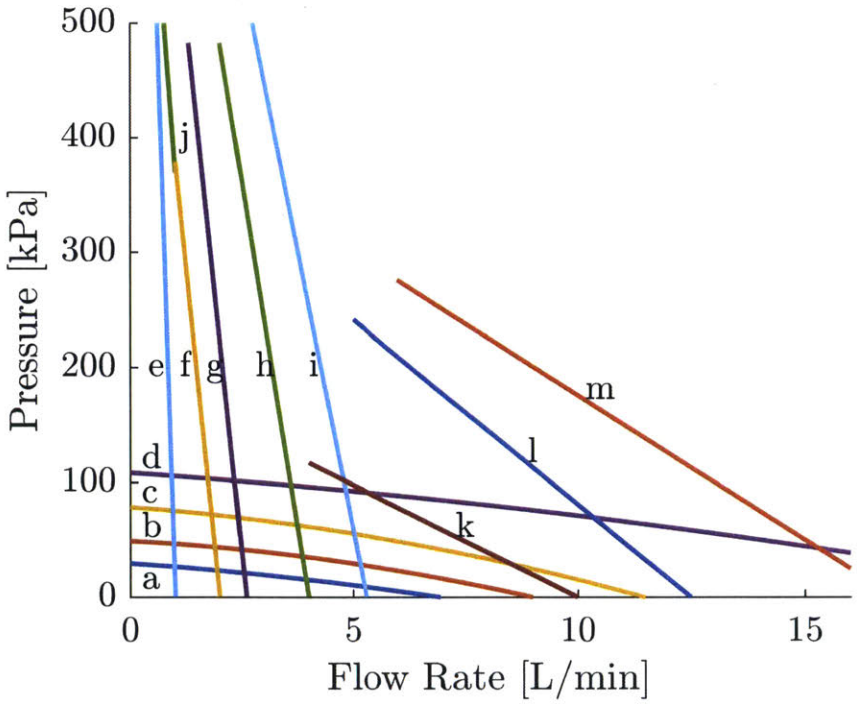

Figure B-1: Pressure-flow relationship of pumps considered in this analysis. See Table B.1 for specifications and cost.

A system pressure-flow curve was produced for each design iteration and compared to 13 DC pump curves (Fig.B-1). With the exception of a-d which are centrifugal pumps, the remainder are diaphragm pumps. The pump, whose intersection point with the system curve most closely provided the design flow-rate, was used for esti-

mating the cost and energy consumption. The pumps were assumed to be operating at their rated power consumption through the full batch duration.

Table B.1: Cost and Power Specifications for Pumps

#	**Manufacturer**	**Model**	**Power [W]**	**Cost [$]**
a	Topsflo	B10H-B12	11	18
b	Topsflo	B04H	20	19
c	Topsflo	B10-B24	31	19
d	Topsflo	C01-B24	48	45
e	Singflo	100GRO	24	14
f	Singflo	FL-2401	22	16
g	Singflo	FL-2403	24	16
h	Singflo	FL-2402A	31	18
i	Ronda	DP-150	40	54
j	Ronda	DP-130	15	53
k	Singflo	FL-31	36	33
l	Singflo	FL-34	60	34
m	Singflo	FL-44	134	35

Bibliography

[1] WHO/UNICEF. Progress on Sanitation and Drinking Water Supply, 2015 Update and MDG Assessment. Technical report, 2015.

[2] WHO/UNICEF. Drinking Water Equity, Safety and Sustainability. *Joint Monitoring Programme for Water Supply and Sanitation*, page 62, 2011.

[3] David Mckenzie and Isha Ray. Household Delivery Options in Urban and Rural India. Technical Report Working Paper No.224, Stanford University, Stanford, California, 2004.

[4] Ruchira Ghosh, Arun Kansal, and Sakshi Aghi. Implications of end-user behaviour in response to deficiencies in water supply for electricity consumption âĂŞ A case study of Delhi. *Journal of Hydrology*, 536(March 2015):400–408, 2016.

[5] Abdul Shaban and R.N. Sharma. Water Consumption Patterns in Domestic Households in Major Cities Water Required for Different Activities. *Economic and Political Weekly*, (1993):2190–2197, 2007.

[6] P Bajpai and L Bhandari. Ensuring access to water in urban households. *Economic and Political Weekly*, 36(39):3774–3778, 2001.

[7] Igor S. Zektser and Lorne G. Everett. *Groundwater resources of the world and their use*, volume 6. 2004.

[8] Central Pollution Control Board. Status of Groundwater Quality in India. Technical report, 2008.

[9] Bureau of Indian Standards. Indian Standard: Drinking Water Specification (second revision). page IS 10500, 2012.

[10] Vincenzo Bellizzi, Luca De Nicola, Roberto Minutolo, Domenico Russo, Bruno Cianciaruso, Michele Andreucci, Giuseppe Conte, and Vittorio E. Andreucci. Effects of water hardness on urinary risk factors for kidney stones in patients with idiopathic nephrolithiasis. *Nephron*, 81(SUPPL. 1):66–70, 1999.

[11] Central Groundwater Board. Ground Water Quality in Shallow Aquifers of India. Technical report, Government of India, 2010.

[12] Himanshu Kulkarni, Mihir Shah, and P.S. Vijay Shankar. Shaping the contours of groundwater governance in India. *Journal of Hydrology: Regional Studies*, 2015.

[13] The World Bank. Deep Wells and Prudence : Towards Pragmatic Action for Addressing Groundwater Overexploitation in India. Technical report, The International Bank for Reconstruction and Development/The World Bank, Washington, DC, 2010.

[14] Paniit Conclave. Water sector in India : Critical Issues in India. 2010.

[15] World Resources Institute, WBSCD, and Triveni Water Institute Confederation of Indian Industry. India Water Tool.

[16] EurekaForbes. *Aquaguard Geneus*, 2016.

[17] KENT RO Systems Ltd. *Supreme RO*, 2016.

[18] Comprehensive Initiative on Technology Evaluation. Household Water Filter Evaluation. pages 1–31, 2015.

[19] Catherine L O'Connor. *Decentralized Water Treatment in Urban India , and the Potential Impacts of Reverse Osmosis Water Purifiers.* PhD thesis, Massachusetts Institute of Technology, 2016.

[20] Transparency Market Research. Water Purifier Market - India Industry Analysis, Size, Share, Growth, Trends and Forecast 2016 - 2024. Technical report, Albany, NY, 2016.

[21] Natasha C. Wright and Amos G. Winter. Justification for community-scale photovoltaic-powered electrodialysis desalination systems for inland rural villages in India. *Desalination*, 352:82–91, 2014.

[22] Boris Pilat. A Case for Electrodialysis. *International Water & Irrigation*, 7:195–225, 1991.

[23] H. Strathmann. Electrodialysis, a mature technology with a multitude of new applications. *Desalination*, 264(3):268–288, 2010.

[24] REvivED Water Consortium. Low energy solutions for drinking water production by a revival of electrodialysis systems, 2016.

[25] Boris Pilat. Practice of water desalination by electrodialysis. *Desalination*, 139(1-3):385–392, 2001.

[26] Sreekumaran Thampy, Girish R. Desale, Vinod K. Shahi, Babubhai S. Makwana, and Pushpito K. Ghosh. Development of hybrid electrodialysis-reverse osmosis domestic desalination unit for high recovery of product water. *Desalination*, 282(1418):104–108, 2011.

[27] Kishor G Nayar, P Sundararaman, J D Schacherl, C L O'Connor, Michael L Heath, Mario O Gabriel, Sahil R Shah, Natasha C. Wright, and Amos G Winter V. Feasibility Study of an Electrodialysis System for In-Home Water Desalination in Urban India. *Development Engineering*, 2:38–46, 2016.

[28] World Health Organization. *Guidelines for Drinking-Water Quality.* Geneva, 4th edition, 2011.

[29] Mohtada Sadrzadeh, Anita Kaviani, and Toraj Mohammadi. Mathematical Modeling of Desalination By Electrodialysis. In *Tenth International Water Technology Conference*, pages 221–233, Alexandria, Egypt, 2006.

[30] J. M. Ortiz, J. a. Sotoca, E. Expósito, F. Gallud, V. García-García, V. Montiel, and a. Aldaz. Brackish water desalination by electrodialysis: Batch recirculation operation modeling. *Journal of Membrane Science*, 252(1-2):65–75, 2005.

[31] Yoshinobu Tanaka. A computer simulation of batch ion exchange membrane electrodialysis for desalination of saline water. *Desalination*, 249(3):1039–1047, 2009.

[32] Marcello Fidaleo and Mauro Moresi. Optimal strategy to model the electrodialytic recovery of a strong electrolyte. *Journal of Membrane Science*, 260(1-2):90–111, 2005.

[33] Zahra Zourmand, Farzaneh Faridirad, Norollah Kasiri, and Toraj Mohammadi. Mass transfer modeling of desalination through an electrodialysis cell. *Desalination*, 359:41–51, 2015.

[34] MATLAB. *version 8.6.0 (R2015b).* Natick, Massachusetts, 2010.

[35] Yoshinobu Tanaka. *Ion Exchange Membrane Electrodialysis: Fundamentals, Desalination, Separation.* Nova Science Publishers, 2010.

[36] G. Kortum. *Treatise on Electrochemistry.* Elsevier Publishing Company, 1965.

[37] Sylwin Pawlowski, João G. Crespo, and Svetlozar Velizarov. Pressure drop in reverse electrodialysis: Experimental and modeling studies for stacks with variable number of cell pairs. *Journal of Membrane Science*, 462:96–111, 2014.

[38] Francesco Nicolò Ponzio, Alessandro Tamburini, Andrea Cipollina, Giorgio Micale, and Michele Ciofalo. Experimental and computational investigation of heat transfer in channels filled by woven spacers. *International Journal of Heat and Mass Transfer*, 104:163–177, 2017.

[39] Willi H. Hager. *Wastewater Hydraulics - Theory and Practice.* Springer-Verlag Berlin Heidelberg.

[40] Matthias Johannink, Kannan Masilamani, Adel Mhamdi, Sabine Roller, and Wolfgang Marquardt. Predictive pressure drop models for membrane channels with non-woven and woven spacers. *Desalination*, 376:41–54, 2015.

[41] CONWED Global Netting Solutions, Minneapolis, USA. *Reverse Osmosis Feed Spacers*, 2016.

[42] Industrial Netting, Minneapolis, USA. *Woven Nylon, Polyester, or Polypropylene Plastic Mesh*, 2016.

[43] Georges Belfort and Gerald A Guter. Hydrodynamic Studies for Electrodialysis. Technical report, McDonnell Douglas Corporation, Newport Beach, California, 1969.

[44] G. Schock and A. Miquel. Mass transfer and pressure loss in spiral wound modules. *Desalination*, 64(C):339–352, 1987.

[45] C. P. Koutsou, S. G. Yiantsios, and A. J. Karabelas. Direct numerical simulation of flow in spacer-filled channels: Effect of spacer geometrical characteristics. *Journal of Membrane Science*, 291(1-2):53–69, 2007.

[46] L. Gurreri, A. Tamburini, A. Cipollina, G. Micale, and M. Ciofalo. Flow and mass transfer in spacer-filled channels for reverse electrodialysis: a CFD parametrical study. *Journal of Membrane Science*, 497:300–317, 2016.

[47] Piotr Długołecki, Benoît Anet, Sybrand J. Metz, Kitty Nijmeijer, and Matthias Wessling. Transport limitations in ion exchange membranes at low salt concentrations. *Journal of Membrane Science*, 346(1):163–171, 2010.

[48] PCA GmbH. PC*Cell* ED 64 0 02 Technical Description. page 1, 2016.

[49] PCA GmbH. PCA Ion Exchange Membranes: Technical Data Sheet. page 1, 2016.

[50] M. S. Isaacson and Ain a. Sonin. Sherwood Number and Friction Factor Correlations for Electrodialysis Systems, with Application to Process Optimization. *Industrial & Engineering Chemistry Process Design and Development*, 15(2):313–321, 1976.

[51] E. Brauns, W. De Wilde, B. Van den Bosch, P. Lens, L. Pinoy, and M. Empsten. On the experimental verification of an electrodialysis simulation model for optimal stack configuration design through solver software. *Desalination*, 249(3):1030–1038, 2009.

[52] J. Uche, F. Círez, A. A. Bayod, and A. Martínez. On-grid and off-grid batch-ED (electrodialysis) process: Simulation and experimental tests. *Energy*, 57:44–54, 2013.

[53] Laura J. Banasiak, Thomas W. Kruttschnitt, and Andrea I. Schäfer. Desalination using electrodialysis as a function of voltage and salt concentration. *Desalination*, 205(1-3):38–46, 2007.

[54] Ronan K. McGovern, Syed M. Zubair, and John H. Lienhard V. Design and Optimization of Hybrid ED-RO Systems for the Treatment of Highly Saline Brines. In *International Desalination Association World Congress*, Tianjin, China, 2013.

[55] Hong Joo Lee, F. Sarfert, H. Strathmann, and Seung Hyeon Moon. Designing of an electrodialysis desalination plant. *Desalination*, 142(3):267–286, 2002.

[56] F. S. Rohman and N. Aziz. Optimization of batch electrodialysis for hydrochloric acid recovery using orthogonal collocation method. *Desalination*, 275(1-3):37–49, 2011.

[57] Reliance Energy. MERC Multi Year Tariff Order for FY 2016-17 to FY 2019-20. Technical report.

[58] Baoji Changli Special Metal Co. Ltd., Shaanxi, China. *Platinized Titanium Anode*, 2014.

[59] Hangzhou Iontech Environmental Co. Ltd., Zhejiang, China. *IONSEP Membranes*, 2014.

[60] Weihai Cortec International Trade Co. Ltd., Shandong, China. *Plastic Spacer for RO Membrane Rolling*, 2015.

[61] Natasha Wright, Sahil Shah, and Amos G. Winter. Modeling of Electrodialysis and Validation at Small and Large Scales (In Preparation). *Desalination*, ?, 2017.

[62] P.H. Gleick. Basic Water Requirements for Human Activities: Meeting Basic Needs. Water International. *Water International*, 21:83–92, 1996.

[63] K. Deb and T Goel. Controlled Elitist Non-dominated Sorting Genetic Algorithms for Better Convergence. In *Lecture Notes in Computer Science*, pages 67–81. Springer Berlin Heidelberg.

[64] M Srinivas and L.M Patnaik. Adaptive probabilities of crossover and mutation in genetic algorithms. *IEEE Transactions on Systems, Man, and Cybernetics*, 24:4:656–667, 1994.

[65] K. Deb, A. Pratap, Agarwal S., and T. Meyarivan. A Fast and Elitist Multiobjective Genetic Algorithm: NSGA-II. *IEEE Transactions on Evolutionary Computation*, 6:2:182–197, 2002.

[66] Ronan K. McGovern, Syed M. Zubair, and John H. Lienhard V. The cost effectiveness of electrodialysis for diverse salinity applications. *Desalination*, 348:57–65, 2014.

[67] Younggy Kim, W. Shane Walker, and Desmond F. Lawler. Electrodialysis with spacers: Effects of variation and correlation of boundary layer thickness. *Desalination*, 274(1-3):54–63, 2011.

[68] Ji-Hee Min and Han-Seung Kim. Effect of operating conditions on the treatment of brackish groundwater by electrodialysis. *Desalination and Water Treatment*, 51(January 2015):5132–5137, 2013.

[69] Marc A. Anderson, Ana L. Cudero, and Jesus Palma. Capacitive deionization as an electrochemical means of saving energy and delivering clean water. Comparison to present desalination practices: Will it compete? *Electrochimica Acta*, 55(12):3845–3856, 2010.